Transcription coactivator OCA-B/Pou2af1 is necessary and sufficient to promote T cell-intrinsic CD4 memory

Wenxiang Sun[1,2,¶,$], Heejoo Kim[1,2,Ψ,$], Jelena Perovanovic[1,2,§], Erik Hughes[1,2], Junhong Du[1,2], Andrea Ibarra[1,2], J. Scott Hale[1], Matthew A. Williams[1,2], Dean Tantin[1,2,3,*]

[1]Department of Pathology, University of Utah School of Medicine, Salt Lake City, UT 84112, U.S.A.

[2]Huntsman Cancer Institute, University of Utah School of Medicine, Salt Lake City, UT 84112, U.S.A.

[3]Lead contact

[*]Correspondence: dean.tantin@path.utah.edu

[$]Equal contributors

[¶]Current address: Sumitomo Dainippon Pharma Oncology, 3900 N. Traverse Mountain Blvd., Suite 100, Lehi, Utah 84043

[Ψ]Current address: Janssen Research & Development, LLC., Neuroimmunology Drug Discovery, 3210 Merryfield Row, San Diego, CA 92121.

[§]Current address: Recursion Pharmaceuticals, 41 400 W, Salt Lake City, UT 84101

Characters in title (including spaces): 128

Words in abstract: 218

Character count (including spaces, excluding references): 63,307

Total main figures and tables: 6

In brief eTOC blurb

Sun et al. use T cell conditional knockout and ectopic expression to show that OCA-B is required for, and sufficient to promote, $CD4^+$ memory T cell formation in vivo. Using fluorescent reporter mice, they show that OCA-B expression can be used to prospectively identify effector T cells with enhanced memory potential.

Highlights

- **Ectopic OCA-B expression is sufficient to promote Th1 memory**
- **OCA-B controls the expression of genes in responding $CD4^+$ T cells that regulate effector response and memory**
- **OCA-B expression can be used to prospectively identify $CD4^+$ memory precursor cells**
- **OCA-B expression is reduced after memory cells are formed**

SUMMARY

The molecular mechanisms leading to the establishment of durable immunological memory are inadequately understood, limiting the development of effective vaccines and durable anti-tumor immune therapies. Using a T cell-conditional knockout mouse model and a viral pathogen, we show that expression of the transcription cofactor OCA-B (Pou2af1/Bob.1/OBF-1) within T cells is necessary for proper $CD4^+$ memory T cell formation. We also show that ectopic OCA-B expression is sufficient to drive T cells towards a memory fate, while having minimal effects on primary antiviral effector response. Bulk and single-cell gene expression profiling comparing cells transduced with OCA-B and empty vector at primary effector response identifies changes in gene expression consistent with later memory formation, including genes increased (*Tbx21*, *Il7r*, *Gadd45b*, *Socs2*) in specific subpopulations by ectopic OCA-B expression. Short-lived effector T cell compartments are expanded but show increased expression of *Gadd45b* and *Socs2*, while clusters of effector cells with memory potential show increased expression of *Bcl2*, *Il7r*, *Tcf7* and *Slamf6*. We also describe an OCA-B-mCherry reporter mouse allele that selectively labels B and T lymphocytes, and shows high reporter expression in $CD4^+$ T_{CM} cells. We show that elevated OCA-B expression prospectively identifies cells with increased survival capability and memory recall potential. Cumulatively, the results demonstrate that OCA-B is necessary and sufficient to promote CD4 T cell memory in vivo.

Introduction

The ability to respond robustly to secondary antigen exposures ("immunological memory") is a defining feature of the adaptive immune system and forms the physiologic basis for vaccination(Sallusto et al., 2010). Immunological memory not only provides critical protection against pathogens, but can also drive autoimmune and anti-tumor responses (Cafri et al., 2019; Chee et al., 2014; Elyaman et al., 2008; Hurton et al., 2016; Kawakami et al., 2005; Raphael et al., 2020; Rosato et al., 2019; Yeo et al., 2018). Central memory T cells (T_{CM}), which home to secondary lymphoid organs, are particularly long-lived and demonstrate high proliferative capacity upon stimulation. In $CD4^+$ T cells, where the molecular basis of memory remains incompletely defined, the transcriptional co-regulator OCA-B (also known as Bob.1, OBF-1 and Pou2af1) (Luo and Roeder, 1995; Strubin et al., 1995) is mostly silent in naïve T cells, but becomes induced upon stimulation (Sauter and Matthias, 1997; Zwilling et al., 1997). OCA-B docks with its cognate transcription factor Oct1/Pou2f1 to regulate T cell target genes (Shakya et al., 2015). In vitro, OCA-B's effects on target gene expression are maximal after withdrawing the stimulus, then resting and re-stimulating T cells (Shakya *et al.*, 2015). OCA-B mediates these effects at least in part by recruiting histone lysine demethylases such as Jmjd1a (Kdm3a, Jhdm2a) to remove inhibitory histone methylation modifications at silent but previously activated target loci (Shakya *et al.*, 2015).

In mice, OCA-B expression can be detected, varying over a 10-fold range, in responding cells one day after infection with lymphocytic choriomeningitis virus (LCMV) (Shakya *et al.*, 2015). Germline OCA-B deletion results in normal primary T cell responses to LCMV, but severely attenuates $CD4^+$ memory T cell formation and recall response. Elevated levels of *Ocab* (*Pou2af1*) mRNA are seen in $CD4^+CD25^{lo}$ early effector cells that are enriched for the ability to form memory after viral clearance (Snook et al., 2018). T cell-specific OCA-B knockout using a conditional mouse allele strongly attenuates spontaneous autoimmune diabetes, with autoreactive TCR specificities in pancreas either deleted or associated with anergy (Kim et al., 2021). Cumulatively, these findings demonstrate potent roles for OCA-B in antigen recall response, immune memory and autoimmunity.

Here, we use a conditional *Pou2af1* (*Ocab*) mouse allele to test T cell-intrinsic effects of OCA-B deletion on $CD4^+$ central memory formation and recall responses. We find that OCA-B deletion in T cells reduces memory responses while leaving primary timepoints unaffected. OCA-B deficient cells that do respond to secondary infection show defects in IFNγ expression, reverting to levels observed in the initial infection. Using retroviral transduction of primary T cells, we show that ectopic OCA-B expression does not alter effector cell numbers at 8 days post-infection (peak T cell response to LCMV), but is sufficient to expand the memory recall effector pool at the expense of empty vector-transduced controls. The effect becomes progressively stronger at later timepoints. mRNA expression profiling of effector cells, using both bulk and single-cell RNA-seq approaches, reveals changes in

genes associated with effector and memory properties, signaling and homing in cells ectopically expressing OCA-B. These include global increases in *Socs2* and *Gadd45b*, expansion of short-lived terminal effector T cell populations, and increases in *Tcf7* and *Il7r* in specific OCA-B-transduced memory precursor populations. Finally, we generated an OCA-B-3×mCherry reporter knock-in mouse allele. This allele efficiently labels B cell populations in different compartments such as bone marrow, spleen and peritoneal cavity. Although they have 10-100-fold less fluorescence relative to B cells, in the homozygous condition this allele efficiently labels T cells. Unexpectedly, reporter mice mark rare populations of T cells in the thymus, and naïve $CD4^+$ T cells with some degree of OCA-B expression. We find that $CD62L^{hi}CD44^{hi}$ T_{CM} cells have higher frequencies and levels of OCA-B expression compared to naïve cells. Using this reporter to chart OCA-B expression in T cells in response to $LCMV^{Arm}$, we show that OCA-B expression is maximal in antigen-specific memory cells and unexpectedly declines upon rechallenge. Finally, we show that elevated endogenous OCA-B expression prospectively identifies $CD4^+$ T effector cells responding to LCMV with enhanced survival capability and expansion potential following viral rechallenge.

Star Methods

"Key resources" table [uploaded separately]

Resource availability

Lead contact

Further information and requests for resources and reagents should be directed to and will be fulfilled by the lead contact, Dean Tantin (dean.tantin@path.utah.edu).

Materials availability

The MSCV-GFP-OCA-B plasmid and OCA-B-3×mCherry reporter mice are available upon request from the Lead Contact with a completed Materials Transfer Agreement.

Data and code availability

This manuscript does not report original code.

Experimental model and subject details

Laboratory mice

All mice used in this study were on the C57BL6/J strain background. All animal experiments were approved by the University of Utah Institutional Animal Care and Use Committee (17-05008). *Pou2af1* (*Ocab*) conditional (floxed) mice were described previously (Kim *et al.*, 2021). *Pou2af1*-3×mCherry reporter knock-in mice were generated on a C57BL/6N background (Biocytogen), but all subsequent mouse crosses (>5 prior to generation of data herein) were to C57BL/6J.

Method details

LCMV and *Listeria* infection

LCMV Armstrong 53b ($LCMV^{Arm}$) (Ahmed et al., 1984) was grown in BHK cells and titered using Vero cells (Oxenius et al., 1998). For primary infection, 8-to 12-week-old $Ocab^{fl/fl}$ or $Ocab^{fl/fl}$;CD4-Cre mice were inoculated i.p. with 2×10^5 plaque-forming units (PFU) of $LCMV^{Arm}$. For heterologous rechallenge with *Listeria monocytogenes* expressing LCMV glycoprotein 61-80 (Lm-gp61) (Shen et al., 1995), bacteria were grown in log phase in BHI media, and concentrations were calculated using OD at 600 nm (OD of 1=1×10^9 CFU/mL). Mice were rechallenged intravenously with 2×10^5 colony forming units (CFU) of Lm-gp61 the indicated number of days after primary infection as published (Kim et al., 2012).

Bone marrow radiation chimeras

140 Radiation chimeras were generated as published (Mitchell et al., 2010). Briefly, male Ly5.1 C57BL/6J
141 mice were used as recipients. Mice received a split dose of 900 Rad (2×450 RAD, spaced 1 hr apart),
142 and were engrafted one day later with 1 million mixed donor bone marrow cells. Competitor bone
143 marrow cells from Ly5.2/Thy1.1 but otherwise wild-type mice, and experimental cells from
144 Ly5.2/Thy1.2 *Ocab*$^{fl/fl}$ or littermate *Ocab*$^{fl/fl}$;CD4-Cre mice, were isolated from femurs and tibias of
145 donor mice. After red blood cell lysis, CD3^{+} cells were depleted using biotinylated anti-CD3 antibodies
146 (eBioScience) and anti-biotin magnetic MicroBeads (Miltentyi Biotech) according to the
147 manufacturer's instructions. CD3-depeleted bone marrow cells were mixed 1:1 and injected retro-
148 orbitally. The chimeras were rested for 8 weeks to allow engraftment, after which mice were infected
149 as above. Virus-reactive cells were identified by LCMVgp$_{66–77}$:I-Ab tetramer staining.
150

151 **pMSCV-IRES-GFP-OCA-B vector generation**

152 Wild-type *Ocab* cDNA was amplified from the plasmid pcDNA3.1-OCA-B (Luo and Roeder, 1995) (a
153 gift from Robert Roeder, Rockefeller University) by PCR and cloned into the pMSCV-IRES-GFP
154 (pMIGR1) retroviral vector (a gift from Ryan O'Connell, University of Utah). Primers used for
155 amplification were mOcab-F-XhoI, 5'CTCGAGCTGTCTGCTTCAAAGAGAAAAGGCAAC; mOcab-R-
156 *Eco*RI, 5' GAATTCCTAAAAGCCCTCCACGGAGAGGGT. The PCR product was gel purified,
157 digested with *Eco*RI and *Xho*I, and inserted into a similarly digested pMIGR1 backbone using T4 DNA
158 ligase to generate pMIG-OCA-B. All constructs were validated by resequencing.
159

160 **CD4^{+} T cell isolation and stimulation**

161 Naïve splenic CD4^{+} T cells were isolated and simulated as described previously (Shakya et al., 2011).
162 Briefly, spleens were dissociated by grinding and passing through a 70 μm nylon strainer. Red blood
163 cells were lysed by ACK lysis buffer (150 mM NH_4Cl, 10 mM $KHCO_3$, 0.1 mM EDTA). Cells were
164 isolated from mice using a naïve CD4^{+} T cell isolation kit (Miltenyi), and stimulated in culture using 10
165 μg/mL plate-bound anti-CD3ϵ and 2 μg/mL anti-CD28 antibodies (eBioscience).
166

167 **Ectopic OCA-B expression in CD4^{+} T cells**

168 T cells from Ly5.1 SMARTA and Thy1.1 SMARTA mice were purified using a CD4^{+} T cell isolation kit
169 (Miltenyi). Cells were placed into RPMI 1640 medium supplemented with 10% fetal bovine serum, 50
170 U/mL penicillin, 50 μg/mL streptomycin, 2 mM L-glutamine, 1 mM sodium pyruvate, 1× MEM
171 nonessential amino acids, 55 μM 2-mercaptoethanol, and 20 IU/mL recombinant human IL-2. All
172 components were from ThermoFisher with the exception of IL-2, which was supplied by R&D
173 Systems. Cells were simultaneously transduced with pMIGR retroviruses packaged in 239T cells, with
174 or without expressed mouse OCA-B cDNA, using spin infection. For spin infection, cells were

175 centrifuged with 293T retroviral supernatant at 1000×*g* for 2 hr at 37°C in the presence of 4 μg/mL
176 polybrene (Sigma). On the following day, transduced GFP^+ cells were isolated by fluorescent-
177 activated cell sorting. 2×10^4 pMIGR1- and pMIGR1-OCA-B-transduced cells were combined and co-
178 transferred into wild-type (Ly5.2/Thy1.2) C57BL6/J mice. Chimeric mice were infected with $LCMV^{Arm}$
179 and re-challenged with Lm-gp61 as described above.
180
181 **Flow cytometry**
182 Spleens were dissociated and passed through a 70 μm nylon strainer. Red blood cells were lysed by
183 ACK lysis buffer (150 mM NH_4Cl, 10 mM $KHCO_3$, 0.1 mM EDTA). For intracellular staining, cell
184 suspensions in RPMI supplemented with 10% fetal bovine serum were re-stimulated for 4 hr with 1
185 μM LCMV $GP_{61–80}$ or 0.1 μM GP_{33-41} peptide along with Brefeldin A (GolgiPlug Becton-Dickinson, 1
186 μl/mL) as published (Murali-Krishna et al., 1998; Williams et al., 2008). Cells were subsequently fixed
187 by cell fixation/permeabilization solution (Cytofix/Cytoperm, Becton-Dickinson) according to the
188 manufacturer's protocol. For tetramer staining, APC-conjugated $gp_{66–77}$:I-A^b and gp_{33-41}:H-$2D^b$
189 tetramers were provided by the NIH Tetramer Core Facility (Emory Vaccine Center). Cell suspensions
190 were incubated at 37°C for 3 hr in RPMI with the tetramer followed by cell-surface staining. Tetramer
191 fluorescence was normalized with isotype tetramer (hCLIP:I-A^b) staining. Antibodies used for flow
192 cytometry are presented in the Key Resources Table.
193
194 **Bulk RNAseq**
195 $CD4^+$ T cells were purified from female Ly5.1 SMARTA and Ly5.1/5.2 SMARTA mice, and separately
196 transduced with pMIG-OCA-B or empty vector (EV), respectively. On the following day, transduced
197 GFP^+ cells were sorted, 20,000 of each combined 1:1, and injected intravenously into 24 male
198 C57BL/6J male recipients. 24h later, each recipient mouse was injected intraperitoneally with $2x10^5$
199 pfu $LCMV^{Arm}$. After eight days, the 24 mice were divided into six groups of four mice by combining four
200 spleens together. $CD4^+$ T cells were purified using a Miltenyi CD4 T cell isolation kit. Cells then were
201 stained with PerCP-Cy5.5 Ly5.1 and AF700 Ly5.2 antibodies. $GFP^+Ly5.1^+Ly5.2^+$ (EV) and
202 $GFP^+Ly5.1^+$ (OCA-B-expressing) cells were sorted by fluorescence-activated cell sorting (FACS) and
203 used for RNA purification (RNeasy Mini Kit, QIAGEN). RNA concentrations were determined using a
204 Quant-iT RNA assay kit and a Qubit fluorometer (ThermoFisher). Because limited RNA from EV-
205 transduced cells was obtained, the six EV samples were combined into three samples. One of the six
206 OCAB OE sample failed. Therefore, three EV-transduced and five OCA-B-transduced samples were
207 eventually submitted for RNAseq analysis. Total RNA samples (200-500 ng) were hybridized with
208 Ribo-Zero Plus (Illumina) to deplete cytoplasmic and mitochondrial and ribosomal RNA from samples.
209 RNA sequencing libraries were prepared as described using the Stranded Total RNA Prep, Ligation

210 with Ribo-Zero Plus kit (Illumina) and IDT for Illumina RNA UD Indexes Set A, Ligation (Illumina).
211 Purified libraries were qualified on an Agilent Technologies 2200 TapeStation using a D1000
212 ScreenTape assay. The molarity of adapter-modified molecules was defined by qPCR using the Kapa
213 Biosystems Kapa Library Quant Kit. Individual libraries were normalized to 0.65 nM in preparation for
214 Illumina sequence analysis. Sequencing libraries were chemically denatured and applied to an
215 Illumina NovaSeq flow cell using the NovaSeq XP workflow (20043131). Following transfer of the flow
216 cell to an Illumina NovaSeq 6000 instrument, a 150 x 150 cycle paired-end sequence run was
217 performed using a NovaSeq 6000 S4 reagent Kit v1.5 (Illlumina).
218
219 **Bulk RNA-seq analysis**
220 Bulk RNA-seq analysis was performed as previously described (Perovanovic et al.). Briefly, Reads
221 were aligned to *Mm10* using STAR (v2.7.3a) and checked for quality using multiqc (v1.10). Between
222 12 and 14 million pair-end reads were generated for each sample, with >98% of aligned reads
223 mapping to the correct strand and >93% of the reads uniquely aligned to the gene. Differentially
224 expressed genes were identified using DESeq2 version 1.24.0 (Love et al., 2014) with a 5% FDR
225 cutoff. Features with zero counts and 5 or fewer reads in every sample were removed from the
226 analysis. Genes increased by 1.4-fold or more or decreased by 2-fold or more, and with adjusted
227 $p<0.05$ were selected as differentially expressed ($0.5 < \log2FC < -1$; padj ≤ 0.05). Figures were
228 generated in R version 4.0.0 using functions from ggplots libraries and pheatmap.
229
230 **Single-cell RNA-seq**
231 To profile gene expression at the single-cell level, splenic $GFP^+Ly5.1^+Ly5.2^+$ (EV-transduced) and
232 $GFP^+Ly5.1^+$ (OCA-B-transduced) SMARTA cells were collected similarly as for bulk RNA-seq. Cells
233 were resuspended in PBS with 0.04% bovine serum albumin (ThermoFisher), and filtered through 40
234 μm strainers. Viability and cell count were assessed using a Countess II (ThermoFisher). Equilibrium
235 to targeted cell recovery of 6,000 cells along with Gel Beads and reverse transcription reagents were
236 loaded to Chromium Single Cell A to form Gel-bead-in Emulsions (GEMs). Within individual GEMs,
237 cDNA generated from captured and barcoded mRNA was synthesized by reverse transcription at
238 53°C for 45 min. Samples were then heated to 85°C for 5 min. Single cell transcriptomes were
239 assessed using a 10X Genomics Chromium Single Cell Gene Expression instrument. Individual cells
240 were tagged with 16 bp barcodes, and specific transcripts with 10 bp Unique Molecular Identifiers
241 (UMIs) according to manufacturer instructions.
242
243 **Single-cell RNA-seq analysis**

244 Single cell transcriptome data were analyzed and clustered as described previously (Perovanovic *et*
245 *al.*). Sequences from the Chromium platform were de-multiplexed and aligned using CellRanger ver.
246 3.1.0 (10X Genomics) with default parameters mm10-3.0.0. Clustering, filtering, variable gene
247 selection and dimensionality reduction were performed using Seurat ver.4.0.4 (Stuart et al., 2019)
248 according to the following workflow: 1, Cells with <200 detected genes were excluded further analysis.
249 2, Cells with <5% UMIs mapping to mitochondrial genes and *Cd44* expression >0 were retained for
250 downstream analysis. 3, The UMI counts per ten thousand were log-normalized for each cell using the
251 natural logarithm. 4, Variable genes (2000 features) were selected using the FindVariableFeatures
252 function. 5, Common anchors between the conditions were identified using FindIntegrationAnchors
253 function that were further used to integrate these sets. 6, Gene expression levels in the integrated set
254 were scaled along each gene and linear dimensional reduction was performed. The number of
255 principal components was decided through the assessment of statistical plots (JackStrawPlot and
256 ElbowPlot). 7, Cells were clustered using a shared nearest neighbor (SNN) modularity optimization-
257 based clustering algorithm and visualized using two-dimensional uniform manifold approximation and
258 projection (UMAP). 8, One cluster in each condition marked predominantly by mitochondrial genes
259 (indicative of dying cells) was excluded from the analysis. This resulted in 12,886 empty vector-
260 transduced cells with 45,748 mean reads per cell, and 2,595 median genes per cell. The total number
261 of reads was 589,513,069, with 59.6% mapping to exonic regions. Similarly, there were 11,709 OCA-
262 B-transduced cells with 68,931 mean reads per cell, and 2,668 median genes per cell. Total number
263 of reads was 807,111,486, with 57.4% mapping to exonic regions.
264
265 **Memory progenitor isolation, normalization and transfer**
266 To assess contraction of the effector cells with different OCA-B levels, splenic $CD4^+$ T cells were
267 purified from 8 week-old female Ly5.1/5.2 homozygous knock-in reporter, SMARTA TCR transgenic
268 mice. 2×10^4 SMARTA cells were intravenously injected into 15 male Ly5.2/5.2 C57BL/6J recipients,
269 which were infected intraperitoneally 1 day later with 2×10^5 plaque-forming units of $LCMV^{Arm}$ in 250 μL
270 phosphate-buffered saline. After 8 days, responding $Ly5.1^+5.2^+$ SMARTA T cells were sorted into
271 $mCherry^{hi}$ and $mCherry^{lo}$ populations. Cells were pooled and 8×10^5 $mCherry^{hi}$ and $mCherry^{lo}$ cells
272 were separately injected intravenously into 7 naïve age-matched 9 week-old male C57BL/6J
273 secondary recipients in the case of $mCherry^{lo}$ and 5 secondary recipients in the case of $mCherry^{hi}$.
274 After 8 additional days, mice were sacrificed and splenic $Ly5.1^+5.2^+$ SMARTA cells were counted by
275 flow cytometry. To assess proliferative responses to rechallenge, 15 similar virus-naïve secondary
276 recipients were rested for 43 days post-infection prior to isolation of $mCherry^{hi}$ and $mCherry^{lo}$
277 populations. 1.3×10^4 SMARTA cells were transferred into naïve recipients, which were infected with
278 LCMV one day later. 7 days post-infection, splenic $CD4^+Ly5.1^+5.2^+$ SMARTA cells were evaluated by

279 flow cytometry. Mice with poor infection/response (total splenocyte count $<6\times10^7$) were excluded from
280 the analysis.
281
282 **Quantification and statistical analysis**
283 Excel (Microsoft) and Prism (GraphPad) were used for statistics and graphing. Two-tailed Student T-
284 tests were used to ascribe statistical significance unless otherwise indicated. For all figures, *=*p*-
285 value≤0.05; **=*p*≤0.005; ***=p<0.001. All error bars denote ± standard error of the mean.

286 **Results**

287

288 **OCA-B is required for robust CD4$^+$ T cells memory recall responses**

289 We previously used OCA-B whole-body knockout T cells, SMARTA TCR transgenic mice, and mixed
290 adoptive transfer assays to demonstrate that OCA-B is required for robust monoclonal CD4$^+$ T cell
291 memory responses. SMARTA mice express a transgenic TCR specific for an immunodominant CD4$^+$
292 epitope of the LCMV glycoprotein ($GP_{61–80}$) (Oxenius *et al.*, 1998). While *Ocab*$^{-/-}$ SMARTA CD4$^+$
293 effector T cell expansion was equivalent to wild-type, ~50-fold fewer *Ocab*$^{-/-}$ cells populated the
294 memory compartment after re-challenge (Shakya *et al.*, 2015). These experiments were limited by the
295 fact that 1) T cells were subject to effects of development in an OCA-B deficient environment and 2)
296 monoclonal responses were studied. We used a conditional *Ocab* (*Pou2af1*) mouse allele crossed
297 onto a CD4-Cre driver, which efficiently deletes OCA-B in T cells (Kim *et al.*, 2021), to study effects of
298 OCA-B loss during polyclonal LCMV responses. We infected age- and sex-matched *Ocab*$^{fl/fl}$;CD4-Cre
299 and littermate control *Ocab*$^{fl/fl}$ mice with 2×10^5 pfu LCMV^{Arm} intraperitoneally, and measured specific T
300 cell responses using I-A^b/$gp_{66–77}$ tetramer staining. No significant differences in the frequency of
301 positive cells were observed at 8 days post-primary infection (Figure 1A). Rechallenging these mice
302 with *Listeria monocytogenes* expressing the LCMV glycoprotein epitope (Lm-gp61) (Shen *et al.*, 1995)
303 elicited a trending decrease in the frequency of CD4$^+$ I-A^b/$gp_{66–77}$-positive CD4$^+$ T cells undergoing
304 memory recall response in *Ocab*$^{fl/fl}$;CD4-Cre mice (Figure 1A, D40+7). The responding cells showed
305 no change in percentages of IL-2/IFNγ double-producing CD4$^+$ T cells, but a significant decrease in
306 IFNγ single-producers (Figure 1B,C). The same cells showed minimal changes in Inducible T cell co-
307 stimulator (ICOS), PD-1, Ly6C or CD62L expression (Figure S1).

308 The relatively small reductions in frequencies of tetramer-positive CD4$^+$ T cells at recall
309 response may reflect selection for a small percentage of cells escaping OCA-B deletion. Infection of
310 mice with T cell conditional deletion of *Oct1*/*Pou2f1* (which encodes the transcription factor with which
311 OCA-B docks), indicated a strong selection for cells that escape Cre-mediated deletion in antigen-
312 specific CD4$^+$ memory T cells (Shakya *et al.*, 2015). This selection can be circumvented by performing
313 LCMV infections using bone marrow chimeras in which conditional-deficient or control cells are
314 competed against wild-type T cells in the same animals. We generated bone marrow radiation
315 chimeras in which wild-type donors were co-engrafted 1:1 with congenically-marked *Ocab*$^{fl/fl}$;CD4-Cre
316 or control *Ocab*$^{fl/fl}$ cells into the same recipient animals. In this case, a potential competitive
317 disadvantage conferred by OCA-B deficiency can be identified relative to co-transferred wild-type
318 competitors, and relative to control OCA-B sufficient cells carrying the same congenic markers. Bone
319 marrow was depleted of T cells prior to engraftment (see Methods). After 8 weeks to allow
320 engraftment, recipient mice were infected with LCMV^{Arm} (Figure 1D). The ratio of antigen-reactive

321 *Ocab*$^{fl/fl}$ control effector CD4^{+} T cells to wild-type competitor was close to 1:1 at 8 day post-infection.
322 OCA-B deficient (*Ocab*$^{fl/fl}$;CD4-Cre) cells were slightly reduced relative to wild-type competitor
323 (maximum difference 1.6 fold, Figure 1E). To investigate the effects of T cell-specific OCA-B loss on
324 memory recall responses, we rechallenged mice with Lm-gp61. Following rechallenge, the control to
325 wild-type cell ratio remained close to 1:1 at both primary and memory recall response, while wild-type
326 competitor cells were greatly increased at the expense of OCA-B deficient cells specifically at recall.
327 (>8-fold, Figure 1E,F). Therefore, much like T cell-conditional Oct1 deficiency (Shakya *et al.*, 2015), T
328 cell-conditional OCA-B deficiency in bone marrow chimeras results in competitive defects selectively
329 in CD4^{+} T cell memory recall responses.
330
331 **Ectopic OCA-B expression is sufficient to enhance CD4^{+} T cell memory responses in vivo.**
332 To test if ectopic expression of OCA-B is sufficient to induce more robust memory responses in CD4^{+}
333 T cells, we generated an MSCV-IRES-GFP (pMIGR1) vector expressing mouse OCA-B (pMIG-OCA-
334 B). Using this construct, we transduced Thy1.1^{+} SMARTA TCR transgenic donor T cells. In parallel,
335 Ly5.1^{+} (CD45.1^{+}) control SMARTA cells were transduced with empty vector (EV). The cells were
336 mixed 1:1 and adoptively co-transferred into Thy1.2^{+}Ly5.2^{+} recipients as depicted in Figure 2A. NIH-
337 3T3 cells, which express no endogenous OCA-B, efficiently express OCA-B protein when transduced
338 with pMIG-OCA-B (Figure 2B). After transfer, recipient mice were infected with LCMV^{Arm} and the cell
339 populations were detected by flow cytometry using GFP expressed from MSCV and congenic markers
340 from the donor T cells. The host T cells mounted normal responses to LCMV, allowing SMARTA cells
341 to be monitored in the context of a normal host response. At 8 days post-infection, effector EV- and
342 OCA-B-transduced cells expanded equivalently, maintaining the same ratio in both spleen and
343 peripheral blood (Figure 2C and D, D8). Another group of mice were infected with LCMV^{Arm} and
344 allowed to clear the virus and form memory. Recall responses were induced by re-challenge 52 days
345 post-infection using Lm-gp61. At peak T cell response to rechallenge (day 52+7), ~50-fold more OCA-
346 B overexpressing SMARTA cells were present (Figure 2C and D, D52+8). We also tested the effect of
347 OCA-B overexpression on long-term memory by secondary challenge at day 110. In the case of long-
348 term memory recall responses, responding SMARTA T cells were even more strongly skewed
349 towards cells ectopically expressing OCA-B (Figure 2C and D, D110+7), indicating a progressive
350 increase in memory T cell potential with time. Ratios of percentages from multiple mice are quantified
351 in Figure 2E. These results indicate that the OCA-B expression enhances the ability of CD4^{+} T cells to
352 induce memory responses.
353 Effector T cells that are capable of forming memory can be partly distinguished by the
354 expression of specific surface proteins, though the markers are more robust in CD8^{+} than CD4^{+} cells
355 (Laidlaw et al., 2016; Marshall et al., 2011). To investigate how OCA-B overexpression induces more
356 robust memory responses, we characterized the expression of ICOS, programmed cell death protein-

357 1 (PD-1) (PD-1), CD62L (L-selectin) and Ly6C in OCA-B-overexpressing and empty vector control
358 SMARTA cells at 8 days post-infection. GFP$^+$ SMARTA effector T cells were uniformly CD44^{hi} and
359 unchanged by OCA-B expression (Figure 2F). ICOS and PD-1 levels were slightly decreased by
360 OCA-B overexpression. All GFP$^+$ SMARTA T cells were CD62L^{lo}, however expression was slightly
361 decreased in MIGR1-OCA-B-transduced cells compared to EV (Figure 2F and G). Ly6C by contrast
362 was not significantly altered (Figure 2F and G).
363
364 **Ectopic OCA-B expression results in gene expression changes in effector T cells that precede**
365 **and predict enhanced memory.**
366 Although EV- and OCA-B-transduced SMARTA transgenic CD4$^+$ T cells expand equivalently in
367 response to primary LCMV infection, we hypothesized that ectopic OCA-B expression induces gene
368 expression changes in effector cells that promote later memory formation. Because we did not
369 observe large changes in tested surface markers, we profiled gene expression using splenic SMARTA
370 T cells from recipient mice processed and isolated similarly to the cells in Figure 2C. CD4$^+$ cells were
371 first isolated by magnetic isolation, then Ly5.1+/5.2$^+$ and GFP$^+$ cells were further isolated by FACS
372 (see methods). Three EV groups (each comprising 8 mice) and five OCA-B ectopic expression groups
373 (each comprising four mice) were used for bulk RNA-seq, which showed a high degree of
374 concordance (Figure S2A). Using log2 fold-change cutoffs of <-1 (down-regulated) and >0.5 (up-
375 regulated) and adjusted p<0.05, we identified a large set of ~600 down-regulated genes and a smaller
376 group of ~200 up-regulated genes (Table S1).
377 Unsupervised hierarchical clustering identified groups of genes consistently differentially
378 expressed between the two conditions (Figure 3A). Down-regulated genes included *Sell*, which
379 encodes CD62L and which was also down-regulated at the protein level (Figure 2F-G). Down-
380 regulated genes also surprisingly included a number of genes specific to alternative lymphocyte
381 lineages, such as *Bcl6* and *Foxp3*, which encode master transcription regulators of germinal center B
382 cells and Tfh cells and of regulatory T cells respectively. The top up-regulated gene (3.4-fold) was
383 *Ocab* (*Pou2af1*) itself, providing a quality control (Figure 3A,B). Other up-regulated genes were
384 associated with effector T cell activity (*Tbx21*/*Tbet*, *Zeb2*), CD4$^+$ T cell exhaustion (*Ikzf2*/*Helios*),
385 attenuation of T cell signaling and proliferation (*Socs2*, *Gadd45b*) and fatty acid metabolism (*Acacb*).
386 Example tracks for up- and down-regulated genes are shown in Figure 3B and Figure S2B. Gene
387 ontology (GO) analysis of the up-regulated genes identified terms associated with H3K9me3
388 regulation. Down-regulated genes by contrast were strongly associated with H3K27me3 in CD4$^+$ and
389 CD8$^+$ memory T cells (Figure 3C). Because H3K27me3 is a repressive histone modification, the
390 further down-regulation of genes associated with this modification is consistent with promotion of
391 memory phenotypes. ChIP-X Enrichment Analysis (ChEA) (Lachmann et al., 2010) identifies Tp53

392 and Smc3 as factors that also regulate the gene set induced by OCA-B ectopic expression (Figure
393 3D). p53 and SMC3 may therefore also control expression of these genes alongside OCA-B, or could
394 themselves be controlled by OCA-B to mediate gene induction via an indirect mechanism. The
395 complete sets of significant (p<0.05) Molecular Function, Epigenomic Roadmap and ChEA GO terms
396 are shown in Table S2.
397 We intersected the differential gene expression list with prior bulk RNA-seq experiments using
398 isolated naïve T OCA-B germline knockouts stimulated, rested and restimulated in vitro, and with
399 ChIP-seq experiments identifying targets of Oct1 and OCA-B in these cells (Shakya *et al.*, 2015).
400 Although the formats for these experiments were different, we reasoned that the intersection of these
401 gene sets would represent robust regulated genes and direct targets. Only 1.6% of genes (10 of 620)
402 down-regulated by OCA-B ectopic expression relative to empty vector were up-regulated by OCA-B
403 knockout in vitro in the prior study (Table S3). In contrast, a larger percentage of genes increased by
404 OCA-B ectopic expression (10 of 215, 5%) were down-regulated by OCA-B loss in vitro. These were
405 *Tbx21* (*Tbet*), *Zbtb32*, *Gadd45b*, *Socs2*, *Il1rl1*, *Zeb2*, *Tmem159*, *Tnfsf9*, *Sytl3* and *Plekhf1*. For ChIP-
406 seq, we compared the set of 2680 targets co-bound by Oct1 and OCA-B (Shakya *et al.*, 2015) to the
407 620 genes down-regulated by ectopic OCA-B expression. Of these, 43 were identified as direct
408 Oct1/OCA-B targets. Down-regulated direct target genes include *Bcl6*, *Id3*, *Il7r* and *Sell* (*Cd62l*). Of
409 the 215 up-regulated genes, 25 were identified including *Gadd45b*, *Smad3* and *Tbx21* (*Tbet*) and
410 *Zbtb32* (Table S4). Overall, these findings reveal that OCA-B induces complex changes in the
411 expression of key genes in T cells, many of which are direct targets. Some of these are consistent
412 with attenuation of signaling, growth arrest and later memory formation, while others are more
413 consistent with increased effector function and reduced survival. These findings can be explained by
414 the fact that $CD4^+$ T cell effector responses are heterogenous.
415
416 **Single-cell resolution RNA-sequencing identifies putative memory progenitor cells ectopically**
417 **expressing OCA-B.**
418 *Tcf7* is a transcription factor that has been associated with $CD4^+$ T cell memory (Utzschneider et al.,
419 2016). It has been identified as an OCA-B target gene based on prior ChIPseq (Shakya *et al.*, 2015),
420 but was not significantly differentially expressed in bulk RNA-seq. Similarly, *Il7r* encodes a component
421 of IL-7 receptor, a common gamma chain cytokine receptor important for T cell survival that has also
422 been implicated in memory formation (Joshi et al., 2007). This gene is also a direct OCA-B target
423 gene, but counter-intuitively is down-regulated in bulk RNA-seq (Figure 3A). *Zeb2* is associated with
424 effector function in $CD8^+$ T cells (Guan et al., 2018; Omilusik et al., 2015) and was unexpectedly
425 induced (Figure 3A, Table S1). Memory progenitor cells comprise a small proportion of the effector T
426 cell population (Blattman et al., 2002; Joshi *et al.*, 2007; Snook *et al.*, 2018). Because bulk RNA-seq
427 approaches lack the granularity to identify changes in relative sub-populations or in the genes they

428 express, we also performed single-cell RNA-sequencing (scRNA-seq) at D8 post-LCMV^{Arm} infection.
429 Splenic SMARTA TCR transgenic CD4^{+} and GFP^{+} T cells isolated from four pooled mice per condition
430 were isolated as in the bulk RNA-seq, combined and subjected to scRNA-seq. Similar to a published
431 scRNA-seq study using effector SMARTA cells (Ciucci et al., 2019), we filtered the data by requiring
432 *Cd44* gene expression, as SMARTA cells should be uniformly responding to LCMV at this time.
433 Approximately 13,000 and 12,000 empty vector and OCA-B-expressing SMARTA T cells were profiled
434 with an average depth of ~46,000 and ~69,000 reads/cell, respectively (see Methods).
435 Uniform manifold approximation and projection (UMAP) using empty vector-transduced cells
436 revealed a variety of populations (Figure 4A) almost uniformly expressing CD3 cluster genes such as
437 *Cd3e* as well as *Cd4* (Figure S3). Two small clusters (10 and 11) lacked CD3 gene expression and
438 were likely contaminants. Cluster 8 lacked *Cd4*. We used the cluster identity predictor with the
439 ImmGen database, gene expression enrichment for each population relative to the others (Table S5)
440 and PanglaoDB annotation terms to help define the nature of the clusters. Cluster 8 for example was
441 enriched for *Cd8a*, *Prf1*, *Gzmb* and other hallmark cytotoxic T lymphocyte genes, marking these cells
442 as rare CD8^{+} cells. Contaminating clusters 10 and 11 were myeloid in nature.
443 Of the remaining clusters, 1 and 4 for were enriched for genes such as *Ccr7*, *Bcl2*, *Slamf6* and
444 *Tcf7* (both clusters), *Tox* (cluster 1), and *Cxcr5*, *Il7r*, *Icos* and *Cd69* (cluster 4, Table S5). These
445 clusters likely contain memory precursors, with cluster 4 more memory-like than cluster 1. Cluster
446 annotation terms associated with clusters 4 are shown at the bottom of Figure 4A. Cluster 4 identifies
447 "T Memory Cells" as the first term (adj. p=3.4e-9). Cluster 1 was also associated with memory based
448 on annotation terms, albeit more weakly (Table S5 and not shown). Clusters 0, 2 and 6 by contrast
449 were enriched in *Ccl5* (*Rantes*), *Ifng* and *Tbx21*, respectively (Table S5), and likely comprise terminal
450 effectors. Cluster 5 was enriched for genes encoding histones, cyclin-dependent kinases and
451 proliferating cell nuclear antigen (PCNA) and likely represent proliferating effector T cells. Other
452 clusters also contained gene expression hallmarks of effector T cells (Figure 4A, Table S5).
453 UMAP projections of OCA-B-transduced cells resulted in more uniform clustering (Figure 4B).
454 Fewer, more tightly spaced clusters were identified using the same parameters. Like empty vector-
455 transduced SMARTA cells, almost all the cells expressed *Cd3e* and *Cd4* (Figure S3). Only one
456 contaminating myeloid population (Figure 4B, cluster 6) was identified, and unlike empty vector-
457 transduced cells there was no CD8-expressing cluster. The relative lack of rare CD8-expressing cells
458 likely explains the decrease in *Cd8a* and *Cd8b1* gene expression in bulk RNA-seq (Figure 2A).
459 Cluster 0 contained the largest number of cells and was marked by *Zeb2* expression, as well as other
460 short-lived effector cell markers such as *Klrg1* and *Tbx21* (Table S5). In cells transduced with empty
461 vector, *Zeb2* was enriched in rarer effector populations (Figure 4A, cluster 6) and in CD8^{+} cells
462 (cluster 8), explaining the enrichment for this gene in bulk RNA-seq. One difference between the
463 empty vector- vs. OCA-B-transduced effector cell clusters was the selective co-expression of *Socs2*,

464 which encodes an attenuator of T cell signal transduction, only in the OCA-B-transduced condition
465 (Figure 4C). These results suggest an expansion of short-lived (terminal) effector cells in the OCA-B-
466 transduced condition. Similar to cluster 5 of EV-transduced cells, cluster 5 cells in the OCA-B-
467 transduced condition strongly expressed proliferative markers like histones and *Pcna*. Cluster 4 was
468 most equivalent to cluster 7 in empty vector-transduced cells.

469 The remaining cells were more cohesively clustered compared to their empty vector-
470 transduced counterparts and associated with either effector activity (cluster 0, 1, 2) or
471 effector/memory progenitor activity (cluster 3). The top GO term associated with cluster 3 was also "T
472 memory cells" (Figure 4B, bottom). Interestingly, *Ikzf2*, which has been associated with $CD4^+$ T cell
473 exhaustion (Crawford et al., 2014), was not enriched in the memory-associated cluster 3, but was
474 enriched in the equivalent cluster 4 in EV-transduced cells (Table S5). Furthermore, a number of
475 memory-associated genes in the memory progenitor OCA-B-expressing cluster 3 were more strongly
476 expressed compared to equivalent memory progenitor EV-transduced clusters. Genes expressed
477 more frequently in cluster 3 compared to the surrounding clusters included *Tcf7* (99.3% of cells), *Bcl2*,
478 *Il7r* and *Foxo1* (Table S5). *Tcf7* for example was increased by greater than 4-fold in OCA-B cluster 3,
479 but only slightly more than 2-fold in empty vector clusters 1 and 4 (Table S5). *Slamf6* was increased
480 by greater than 3-fold in OCA-B cluster 3, but by less than 2.5-fold in empty vector clusters 1 and 4.
481 *Bcl2* and *Il7r* were similarly more strongly expressed relative to the other clusters in OCA-B-
482 compared to empty vector-transduced cells. *Foxo1* was not over-represented in either of the
483 equivalent empty vector clusters but was enriched in OCA-B cluster 3. Feature plots showing
484 representative genes in the two sets of clusters are shown in Figure 4C. These findings suggest that
485 OCA-B transduced cells in cluster 3, although not increased in numbers, are qualitatively superior to
486 their empty vector-transduced counterparts at forming memory.

487 Clustering empty vector- and OCA-B-transduced cells together allows the relative proportions
488 of cells with common gene expression features to be determined. Clustering together also generated
489 rare clusters of contaminating CD8 T cell and myeloid cells (Figure 4D clusters 7, 8 and 9). Other
490 clusters were enriched for likely effector cells (clusters 0, 1, 4 and 6), proliferating effector cells
491 (cluster 5) and effector cells with memory progenitor potential (clusters 2 and 3). Feature plots for key
492 genes are shown in Figure 4E. Cluster 2, which was associated with expression of genes associated
493 with both effector and memory activity (e.g. *Ifng*, *Zeb2*) harbored greater that 3-fold more cells in the
494 OCA-B expressing condition (33% vs. 10%), however cluster 3 was also associated with memory
495 (e.g., expressing *Tcf7* and *Il7r* at high levels, Figure 4E) yet contained proportionally fewer than half
496 as many cells as controls. Although there were fewer cells in this cluster, analysis of gene expression
497 levels (Figure 4F) showed that *Il7r*, *Zeb2* and *Gadd45b* gene expression were all elevated in this
498 cluster in OCA-B-transduced comparted to empty vector-transduced cells. *Foxo1*, *Tcf7* and *Tox* by

499 contrast were expressed at similar levels. Together these findings identify quantitative and qualitative
500 changes in gene expression and effector T cell populations that predict increased memory potential.
501
502 **OCA-B knock-in reporter mice fluorescently label CD4$^+$ memory T cell populations**
503 To monitor OCA-B expression in viable cells, we used CRISPR/Cas9 to knock 3 mCherry reporter
504 cassettes into the mouse *Pou2af1* (*Ocab*) locus upstream of the 3' UTR. The mCherry cassettes were
505 preceded by P2A elements, allowing for independent translation. *Pou2af1* is compact, spanning just
506 30 kb. The 3' UTR is ~1kb and lacks significant conservation, making it ideal for reporter cassette
507 insertion. The resulting reporter allele contained the mCherry cassettes inserted between the stop
508 codon and the 3' UTR (Figure S4A). A successful heterozygous knock-in founder and a homozygote
509 generated by intercrossing the progeny were confirmed by PCR genotyping (Figure S4B). Both
510 animals retained normal OCA-B protein expression, indicating that reporter knock-in homozygosity
511 does not interfere with endogenous OCA-B protein expression (Figure S4C). We used flow cytometry
512 to identify peripheral blood mCherry-expressing cells from wild-type, heterozygous and homozygous
513 reporter mice. The expression and function of OCA-B are best characterized in B lymphocytes
514 (Betzler et al., 2022; Casellas et al., 2002). OCA-B expression in B cells was readily detectable
515 (Figure S4D,E). T cells formed a slight shoulder in the heterozygous condition, but were also
516 detectable in homozygous mice (Figure S4D,E). We therefore used homozygous mice exclusively to
517 study T cells, and heterozygous mice to perform a brief characterization of B cell populations.
518 We first profiled OCA-B expression in different B cell populations in unchallenged, specific
519 pathogen-free heterozygous reporter mice. Robust mCherry expression could be detected in organs
520 harboring large numbers of developing and mature B cells – bone marrow, peritoneal cavity, spleen
521 and lymph node (Figure S5A). There was relatively little expression by contrast in total thymocytes. In
522 the bone marrow, we used antibodies against IgM and B220 to discriminate developing (Pro/Pre),
523 immature and recirculating B cells. The presence of the reporter allele conferred no major changes in
524 the relative populations (Figure S5B). The largest change was a 30% drop in the relative percentage
525 of developing B cells. This difference was unlikely to be due to decreased OCA-B function, as
526 heterozygous reporter mice express normal levels of OCA-B (Figure S4C) and as whole body OCA-B
527 knockouts do not show major deficits in developing (immature) B cell numbers and at most 2-fold
528 differences in mature B cells (Kim et al., 1996; Nielsen et al., 1996; Schubart et al., 1996). OCA-B
529 expression was readily detected in the three populations (Figure S5B, bottom). Expression was nearly
530 uniform compared to control wild-type mice lacking the reporter allele, except for a small population of
531 immature B cells that lack OCA-B expression. In the peritoneal cavity, we used anti-IgM and anti-
532 B220 and visualize B-1 and B-2 B cells. Again, only small differences in percentages were present
533 (Figure S5C, top). OCA-B expression was largely uniform, and more robust OCA-B expression was
534 detected in B-2 relative to B-1 cells (bottom).

535 Splenic B cells can be partitioned into transitional (immature) and mature populations based
536 on CD93 (AA4.1) staining. We observed no major changes in total transitional splenic B cells, or in
537 T1/2/3 subsets, in heterozygous reporter mice compared to wild-type controls (Figure S5D). The
538 populations expressed OCA-B uniformly and equivalently. Mature splenic B cell populations can be
539 divided into marginal zone, follicular and non-follicular cells based on CD21 and CD23 expression.
540 The relative populations again showed few changes in the presence of the reporter allele, and all
541 three populations expressed OCA-B strongly (Figure S5E). Expression was largely uniform, though
542 there was an unexpected significant population of newly-formed $CD21^{lo}CD23^{lo}$ B cells expressing no
543 OCA-B. These results document strong reporter activity in B cell populations, with the highest level of
544 activity in the more innate-like marginal zone and B-1 B cells. These results indicate that the OCA-B
545 reporter robustly labels B cells, and has negligible effects on their relative abundances.
546 We then characterized OCA-B expression in T cells from unchallenged, specific pathogen-free
547 homozygous reporter mice. Gating out B cells, approximately 5% of thymocytes expressed some level
548 of mCherry (Figure S6A). Nevertheless, reporter thymi show normal distributions of double-positive
549 and CD4/CD8 single-positive cells (Figure S6B), consistent with findings that OCA-B deletion does
550 not affect T cell development (Shakya *et al.*, 2015). mCherry expression could be identified in all
551 CD4/CD8 double-negative, double-positive and single positive compartments, with the highest
552 amounts seen in double-negative and CD8 single-positive cells (Figure S6B). In the spleen, we tested
553 an allelic series of heterozygous and homozygous reporter alleles. As expected, the relative
554 abundance of $CD4^+$ and $CD8^+$ T cells was unaltered (Figure 5A). As expected, splenic B cells robustly
555 and nearly uniformly express mCherry (Figure 5B). $CD4^+$ T cells express detectable amounts of
556 mCherry but at 10- 100-fold lower levels compared to B cells (Figure 5C). Interestingly, a greater
557 proportion of total $CD8^+$ T cells in specific pathogen-free mice expressed OCA-B (Figure S7A).
558 Additionally, the range of mCherry expression was wider in T cells compared to B cells. While B cell
559 intensity varied over a 6-fold range (Figure 5B), T cells in homozygous knock-in mice varied over 50-
560 fold (Figure 5C, right panel and Figure S7A). Peripheral blood T cells varied over a similar range (not
561 shown).
562 We used antibodies against CD62L and CD44 to stratify resting splenic $CD4^+$ and $CD8^+$ cells
563 into naïve, activated/effector and central memory compartments. Unexpectedly, reporter activity could
564 be detected in approximately 7% of naïve ($CD62L^{hi}CD44^{lo}$) cells (Figure 5D). The nature of these cells
565 (e.g., Tregs, recent thymic emigrants) is unknown. A larger fraction of activated $CD62L^{lo}CD44^{hi}$ cells
566 (37%) showed reporter activity, while $CD62L^{lo}$ cells that had not yet up-regulated CD44 showed levels
567 intermediate between naïve and activated. $CD62L^{hi}CD44^{hi}$ T_{CM} cells showed the highest percentage
568 of reporter activity, with half the cells expressing mCherry (Figure 5D). These results indicate that
569 some but not all T_{CM} cells continue to express OCA-B. In addition, mCherry mean fluorescence
570 intensity (MFI) increased as cells progressed from naïve to activated to T_{CM} (Figure S7B). $CD8^+$ T

571 cells showed comparatively higher expression levels in naïve cells, but decreased expression in the
572 activated state and similar expression in T_{CM} cells (Figure 5E).
573
574 **Elevated OCA-B expression prospectively identifies memory precursor CD4$^+$ T cells**
575 We used the reporter mice together with LCMV infection and MHC class I and class II tetramers
576 recognizing immunodominant LCMV epitopes to assess OCA-B responses during infection,
577 subsequent memory formation and rechallenge. Mice were sacrificed at each timepoint to assess
578 mCherry expression splenic T cells. Prior to infection, >90% of cells were naïve CD44^{lo} phenotype,
579 with 13.7% of these cells and 49.5% of the remaining CD44^{hi} cells expressing mCherry (Figure 6A,
580 D0). These results are comparable to Figure 5D. At 8 days post-infection, significant numbers of
581 tetramer-positive effector cells accumulated, and of these 50% were mCherry-positive, similar to
582 tetramer-negative CD44^{hi} cells (D8). Memory timepoint mice showed even higher percentages of
583 mCherry$^+$ cells (D43, 61.6%), though with a lower degree of expression per cell. We also rechallenged
584 these mice with Lm-gp61 to assess antigen recall responses. Interestingly, responding CD44^{hi} CD4$^+$ T
585 cells reduced mCherry positivity compared to resting memory, and high-affinity tetramer-positive cells
586 showed significant mCherry diminution, declining from >60% to <10% positivity (Figure S8A, D42+7).
587 In contrast to CD4$^+$ mCherry reporter T cells, CD8$^+$ reporter T cells showed significant
588 differences. A higher percentage of D0 CD44^{lo} and CD44^{hi} cells express mCherry, and there were
589 detectably higher percentages of tetramer-positive fluorescent cells at day 5, but by day 8 (the peak of
590 the primary T cell LCMV response) mCherry levels were greatly reduced. Memory timepoints also
591 showed reduced levels of mCherry fluorescence in antigen-specific cells relative to CD4$^+$ T cells
592 (Figure S8B). We did not collect data on CD8$^+$ rechallenge because Lm-gp61 does not express the
593 CD8-dominant epitope recognized by H2-D^b LCMV tetramers.
594 To determine if elevated OCA-B levels in T cells responding to LCMV are associated with
595 increased memory potential, we crossed the reporter allele onto a SMARTA TCR transgenic
596 background to fix the TCR specificity and onto Ly5.1 as a means of tracking cells. We then adoptively
597 transferred congenically marked SMARTA cells into recipient animals, infected with LCMV, isolated
598 mCherry^{hi} and mCherry^{lo} cells at day 8 post-infection, and transferred large numbers of cells (8×10^5)
599 into naïve host animals. After 8 days, we isolated splenic CD4+ T cells to assess donor cell
600 frequencies (Figure 6A). Significantly more cells were recovered from recipient animals engrafted with
601 mCherry^{hi} cells, indicating that the rate of loss of these cells is lower than for control mCherry^{lo} cells
602 (Figure 6B,C). Averaged percentages of splenic SMARTA cells in this experiment were trending
603 towards statistical significance but did not reach $p<0.05$ (not shown). Interestingly, the degree of
604 mCherry fluorescence in the cells that did survive was the same in both groups, though with

605 considerably more variance associated with mCherry^{lo} donor cells (Figure 6D) These findings strongly
606 suggest that effector CD4^{+} cells expressing higher levels of OCA-B undergo less cell death.
607 To test the ability of the cells expressing OCA-B to mount superior antigen recall responses,
608 we similarly transferred congenically marked SMARTA cells into recipient animals, infected with
609 LCMV, but isolated mCherry^{hi} and mCherry^{lo} cells at a memory timepoint after viral clearance (day
610 43). Smaller numbers (4×10^{4}) of memory SMARTA cells were then transferred into naïve hosts which
611 were challenged with LCMV and analyzed at day 7 (Figure 6E). Recipient mice engrafted with
612 mCherry^{hi} SMARTA cells and infected with LCMV mounted better recall responses compared to
613 mCherry^{lo} (Figure 6F,G). Again, there was little difference in mCherry fluorescence in the responding
614 cells (Figure 6H), indicating a plasticity in OCA-B expression whereby expression normalizes following
615 antigen re-encounter. Cumulatively, these results indicate that OCA-B expression labels the central
616 memory compartment and can be used to enrich memory progenitor cells prospectively.

617 **Discussion**

618 Immunological memory provides long-lasting protection against chronic and opportunistic infection.
619 Strategies that promote memory have the potential to improve both vaccine efficacy and tumor
620 immunotherapy. Multiple transcription factors and epigenetic regulators have been reported to
621 modulate formation or function of $CD4^+$ and $CD8^+$ T_{CM} cells, including Oct1 and OCA-B (Shakya *et al.*,
622 2015), Blimp1 (Kallies et al., 2009; Rutishauser et al., 2009; Shin et al., 2013), Suv39h1 (Pace et al.,
623 2018), graded levels of T-bet (Joshi *et al.*, 2007; Marshall *et al.*, 2011), co-expressed Tox and TCF1
624 (Utzschneider *et al.*, 2016), Foxo1 (Hess Michelini et al., 2013; Rao et al., 2012), Bcl6 (Ichii et al.,
625 2007; Pepper et al., 2011), Eomes (Banerjee et al., 2010) and ThPOK (Ciucci *et al.*, 2019). Many of
626 these factors appear to function more precisely in $CD8^+$ compared to $CD4^+$ T cells, and additionally
627 none have been shown to be individually sufficient to selectively promote T cell memory formation or
628 function in vivo. Here we show that loss of the lymphocyte-restricted transcription coactivator OCA-B
629 in T cells confers selective defects in CD4 memory recall response and cytokine production, and that
630 ectopic OCA-B expression does not skew primary effector $CD4^+$ T cell numbers, but is sufficient to
631 promote subsequent memory T cell recall responses. Using an OCA-B reporter mouse strain, we
632 show that elevated levels of endogenous OCA-B in effector T cells during the primary response can
633 be used to prospectively identify memory progenitor $CD4^+$ T cells.

634 OCA-B is a transcriptional coregulatory protein named for its strong expression in the B cell
635 lineage. OCA-B binding to immunoglobulin variable region promoters can regulate Ig repertoires
636 (Betzler *et al.*, 2022; Casellas *et al.*, 2002). After B cell activation, OCA-B is essential for the
637 generation of germinal centers and the generation of high-affinity antibodies (Kim *et al.*, 1996;
638 Schubart *et al.*, 1996). The requirement for germinal center formation has been shown to be B cell-
639 intrinsic (Qin et al., 1998). Unlike B cells, developing and naïve $CD4^+$ T cells express negligible
640 amounts of OCA-B. Instead, OCA-B becomes expressed following T cell activation (Shakya *et al.*,
641 2015). Naïve $CD8^+$ cells express OCA-B more strongly compared to $CD4^+$ cells, and expression is
642 further increased upon activation (Kim *et al.*, 2021). OCA-B has been associated with autoimmunity
643 (Ban et al., 2006; Chevrier et al., 2014; Kim *et al.*, 2021; Nakamura et al., 2012).

644 Prior work used T cell-conditional mice deficient in Oct1, the transcription factor with which
645 OCA-B docks, and competitive mixed bone marrow chimeras to identify decreases in memory
646 potential in T cell lacking Oct1 (Shakya *et al.*, 2015). Oct1 conditional mice directly infected with
647 LCMV showed few differences. This was likely due to selection for cells that fail to delete the
648 conditional allele, as significant bias against recombination could be detected in antigen-specific $CD4^+$
649 memory T cells at day 8 post-infection compared to antigen-nonspecific T cells in the same animal.
650 The positive results that were obtained with bone marrow chimeras required *fl/Δ* mice with one allele
651 germline-deleted (Shakya *et al.*, 2015). In contrast to the findings with Oct1, T cell-conditional loss of

652 OCA-B in polyclonal mice directly infected with LCMV^{Arm} results in detectable deficiencies in memory
653 recall responses and IFNγ expression. The finding that direct infection of OCA-B T cell conditional-
654 deficient mice results in stronger phenotypes vis-à-vis Oct1 suggests a more complete deletion of the
655 *Ocab* allele, reduced selection for retention of the undeleted (floxed) allele, and/or stronger biological
656 effects of OCA-B deletion. The latter may include possible Oct1-independent effects of OCA-B. In
657 competitive mixed bone marrow chimera experiments, T cell-conditional OCA-B loss showed severe
658 deficiencies in memory recall responses compared to wild-type competitor bone marrow and
659 compared to littermate *Ocab* conditional bone marrow lacking the Cre driver.
660 Using LCMV-specific SMARTA TCR transgenic mice, we also show that ectopic OCA-B
661 expression promotes CD4^{+} memory T cell recall responses in vivo. In these experiments, OCA-B is
662 ectopically expressed prior to pathogen exposure, and cells accumulate at the expense of empty
663 vector-transduced control cells selectively at memory recall but not primary response timepoints.
664 Although memory is selectively affected, OCA-B mediates changes in responding CD44^{hi} effector
665 cells that are predictive of later memory formation. ICOS, PD-1 and CD62L (L-selectin) were slightly
666 reduced in OCA-B-transduced SMARTA T cells relative to empty vector-transduced cells isolated
667 from the same animals. *Sell*, which encodes CD62L, is a direct OCA-B target gene, as is *Icos*
668 (Shakya *et al.*, 2015). We also performed bulk and single-cell RNA-seq to delineate gene expression
669 changes that may be predictive of later enhanced T_{CM} formation. Bulk RNA-seq identifies a number of
670 genes whose expression was increased in OCA-B- compared to empty vector-transduced
671 populations, including *Gadd45b*, *Socs2* and *Zeb2*. These changes may be sufficient to confer
672 potential increased memory formation, as small advantages compounded over time can result in the
673 large observed effects. *Gadd45b* promotes autoimmune diseases including lupus, psoriasis and
674 arthritis(Liu et al., 2005; Luo et al., 2011; Rodriguez-Jimenez et al., 2021), as well as for strong anti-
675 tumor immune responses(Ju et al., 2009). Also up-regulated is *Acacb*, which is important for fatty acid
676 synthesis. Memory T cells are known to rely on oxidation of fatty acid stores (Michalek et al., 2011;
677 Pearce et al., 2009). ChIP-X Enrichment Analysis identifies Tp53 and Smc3, proteins associated with
678 growth arrest and topological DNA-DNA interactions, as potential regulators of the up-regulated gene
679 set. Other genes were decreased in bulk RNA-seq, including genes associated with H3K27me3 and
680 repressed in memory cells. The further repression of these genes is consistent with the memory
681 advantage conferred by OCA-B expression.
682 A subset of differentially expressed genes correspond to previously identified OCA-B targets
683 based on ChIP-seq results using in vitro stimulation of T cells lacking OCA-B (Shakya *et al.*, 2015).
684 For this analysis, genes down-regulated by OCA-B loss were compared to genes induced by ectopic
685 expression, and the converse. Using this method, better overlap was identified with genes whose
686 expression is reduced by OCA-B loss and increased by ectopic expression compared to the converse.

687 Many of the gene repression events could therefore be indirect, however there are repressed direct
688 OCA-B targets, e.g. *Sell*, which encodes CD62L. Recent findings that OCA-B can also mediate
689 repression as well as activation (Lu et al., 2019) are consistent with this possibility. If the activity of
690 OCA-B switches between activation and repression comparing cells in vitro vs. in vivo, many targets
691 from this analysis would be missed. More work is needed to uncover mechanisms that dictate OCA-B
692 transcription output in T cells.

693 Two other genes associated with T cell survival and memory formation, *Il7r* and *Tcf7* (Joshi *et*
694 *al.*, 2007; Utzschneider *et al.*, 2016), are counterintuitively decreased in bulk RNA-seq. *Il7r* for
695 example encodes a cytokine receptor important for T cell survival. Effector $CD4^+$ T cell populations
696 can manifest heterogeneity, with sub-populations skewed towards later memory formation (Joshi *et*
697 *al.*, 2007; Snook *et al.*, 2018). Increased *Il7r* expression in memory progenitors for example may be
698 obscured in bulk RNA-seq by decreases in the larger populations of terminal effector cells, which may
699 lead to more culling to create greater capacity for memory formation. Consistently, at single-cell
700 resolution, we identified memory-like cell clusters with increased *Il7r* in the background of global
701 down-regulation. The memory advantages conferred by OCA-B cannot be solely mediated by
702 negative factors that cull effector cells, because both T cells ectopically expressing OCA-B and
703 competing cells expressing empty vector would benefit and show equal representation in recall
704 responses. Therefore, other effects of OCA-B must reinforce memory formation in a memory cell-
705 intrinsic manner. Like *Il7r*, *Tcf7* expression is decreased in bulk RNA-seq but increased in likely
706 memory progenitor populations to a higher degree than corresponding populations in cells transduced
707 with empty vector.

708 We generated an OCA-B knock-in mouse reporter allele, and confirmed robust expression in
709 different B cell populations in unchallenged mice. Most B cells were almost uniformly labeled,
710 however there were sub-populations of immature bone marrow and splenic B cells that completely
711 lack OCA-B expression. The nature and significance of these cells is unknown. Expression was
712 highest in marginal zone B cells, which are largely absent in OCA-B knockout mice (Samardzic et al.,
713 2002). We confirm that expression is 50-100-fold lower in T cells overall compared to B cells. Within
714 the $CD4^+$ T cell compartment, increased OCA-B expression as measured by mCherry fluorescence
715 progressively labels greater fractions of naïve, activated and central memory $CD4^+$ cells. Upon LCMV
716 infection, homozygous reporter mice display robust expression of OCA-B, with half of all tetramer-
717 positive $CD4^+$ T cells showing robust mCherry expression. An even greater fraction of splenic
718 tetramer-positive cells show reporter expression at memory timepoints, though fluorescence intensity
719 is lower. This pattern was not recapitulated in $CD8^+$ cells, which showed earlier expression of
720 mCherry and poor induction in both primary effector, memory and memory recall timepoints. This
721 pattern is consistent with prior findings that naïve $CD8^+$ T cells express OCA-B at higher levels
722 compared to naïve $CD4^+$ cells (Kim et al., 2019).

723 These studies have identified a method of prospectively marking viable $CD4^+$ memory
724 precursor effector T cells. Such methods are largely lacking compared to $CD8^+$ T cells, where markers
725 such as IL7R and KLRG1 can be used to identify memory precursor cells (Joshi *et al.*, 2007).
726 Identifying similar markers and transcriptional regulators that define the memory precursor effector
727 $CD4^+$ T cells will promote major advances in understanding the formation of CD4 T cell memory. We
728 isolated OCA-B^{hi} vs OCA-B^{lo} SMARTA transgenic effector $CD4^+$ T cells at 8 days post-infection, which
729 results in roughly equal partitioning of cells into each group. Populations of effector cells with elevated
730 OCA-B expression contracted less in naïve animals, and were better able to mount recall responses
731 to antigenic rechallenge compared to cells with low or absent OCA-B expression. These results
732 indicate that OCA-B reporter activity can be used to prospectively identify live $CD4^+$ effector cells with
733 augmented capacity to form central memory cells. Cumulatively, the results indicate that OCA-B
734 expression within $CD4^+$ T cells is both necessary for, and sufficient to promote, the emergence of T_{CM}.

735 **Abbreviations**

736 ChEA, ChIP-X Enrichment Analysis; EV, empty vector; FACS, fluorescence-activated cell sorting;
737 GEMs, Gel-bead-in EMulsions; ICOS, Inducible T cell co-stimulator; LCMV, lymphocytic
738 choriomeningitis virus; Lm-gp61, *Listeria monocytogenes* expressing LCMV gp61-80; PCNA,
739 proliferating cell nuclear antigen; pMIG, pMSCV-IRES-GFP; scRNA-seq, single-cell RNA-sequencing;
740 T_{CM}, central memory T cell; UMAP, uniform manifold approximation and projection; UMIs, Unique
741 Molecular Identifiers

742 **Declarations**

743

744 **Consent for publication**

745 Not applicable

746

747 **Availability of supporting data**

748 Please contact author for data requests.

749

750 **Competing interests**

751 The sponsors had no role in study design, collection, analysis and interpretation of data, in the writing
752 of the report or in the decision to submit the article for publication.

753

754 **Author's contributions**

755 DT conceived the study and designed experiments, supervised the study, and provided
756 administrative, technical and material support. WS, HK and AI acquired and interpreted the data. JP
757 performed bioinformatic analyses. JSH and MAW provided material and intellectual support. All
758 authors were involved in writing, reviewing and revising the manuscript.

759

760 **Acknowledgements**

761 We thank M. Chandrasekharan for help with graphics. We thank J. Marvin and the University of Utah
762 Health Sciences Center Flow Cytometry Core facility. We thank O. Allen, B. Dalley and the High-
763 Throughput Genomics Core. MHC tetramers were provided by the NIH Tetramer Core Facility
764 (Atlanta, GA). We thank R. Roeder for the mouse OCA-B cDNA and R. M. O'Connell for the pMIGR1
765 plasmid.

766

767 **Funding**

768 This work was supported by NIH grant AI100873 to DT.

769

770 **Figure legends**

771

772 **Figure 1. OCA-B in T cells is required for robust polyclonal memory CD4$^+$ T cell formation and**
773 **cytokine expression following LCMV infection.**

774 A) *Ocab$^{fl/fl}$*;CD4-Cre and control *Ocab$^{fl/fl}$* mice were infected with LCMV^{Arm}, and rechallenged with Lm-
775 gp61 40 days after LCMV infection. Splenic I-A^b/gp$_{66–77}$ tetramer-positive, CD4$^+$CD44$^+$ T cells were
776 analyzed by flow cytometry 8 days after primary infection and 7 days after heterologous rechallenge.
777 n=5 for each group. n.s.=not significant.

778 B) Splenocytes from LCMV-infected *Ocab$^{fl/fl}$*;CD4-Cre or control *Ocab$^{fl/fl}$* mice were restimulated in
779 vitro with gp$_{61-80}$ peptide for 4 hours, and IFNγ and IL-2 expression in CD4$^+$ T cells examined by flow
780 cytometry. Cells were gated based on I-A^b/gp$_{66–77}$ tetramer, CD4 and CD44 positivity. Data from
781 representative animals are shown.

782 C) Mean T cell frequencies of CD4$^+$CD44$^+$IFNγ^+IL-2$^-$ T cells are shown. n=5 for each group.

783 D) Experimental schematic for mixed bone marrow reconstitution and LCMV challenge. Bone marrow
784 cells were depleted of mature T cells prior to engraftment (see methods).

785 E) Flow cytometry plot showing Thy1.1$^+$Ly5.2$^+$ but otherwise genetically wild-type (WT) donor bone
786 marrow cells engrafted 50:50 with Ly5.2$^+$ control cells lacking the Cre driver (*fl/fl*) or experimental T
787 cell-conditional *Ocab$^{fl/fl}$*;CD4-Cre donor cells (*fl/fl*;Cre). Recipient hosts were Ly5.1$^+$. Splenic effector
788 cells were recovered at primary response (D8) or seven days post-rechallenge (D42+7). Cells were
789 gated based on I-A^b/gp$_{66–77}$ tetramer positivity. Example animals are shown.

790 F) Mean wild-type competitor to control of OCA-B deficient T cell ratios are shown. n=3 for each
791 group.

792

793 **Figure 2. Ectopic OCA-B expression enhances CD4$^+$ T cell memory recall responses in vivo.**

794 A) Experimental schematic for OCA-B transduction and T cell mixed adoptive transfer. Ly5.1$^+$
795 SMARTA cells were transduced with pMSCV-IRES-GFP (pMIG) empty vector (EV) and Thy1.1$^+$
796 SMARTA cells were transduced with pMIG expressing mouse OCA-B (pMIG-OCA-B). Following
797 transduction, the two populations of SMARTA cells were combined 1:1, co-transferred into
798 Ly5.2$^+$/Thy1.2$^+$ C57BL6/J recipient mice, and infected with LCMV^{Arm}. Recipients were rechallenged
799 with Lm-gp61 on either day 52 or 110 post-LCMV infection, and in each case analyzed after 7 days.

800 B) Lysates from 3T3 cells transduced with either empty pMIG empty vector (EV) or pMIG-OCA-B
801 were immunoblotted using antibodies against OCA-B. α-tubulin is shown as an internal loading
802 standard.

803 C) Flow cytometric analysis of Ly5.1$^+$ pMIG empty vector-transduced (EV) and Thy1.1$^+$ pMIG-OCA-B-
804 transduced (OCA-B) SMARTA cells in the spleen and blood of a representative recipient mouse at

805 peak effector response (D8), peak memory recall response (52+7) and long-term memory recall
806 (D110+7). Cells were first gated based on CD44, CD4 and GFP positivity.
807 D) Mean relative percentages of splenic and blood total EV- or pMIG-OCA-B-transduced (GFP^+)
808 SMARTA cells were plotted at D8, D52+7 and 110+7. Each datapoint represents an individual mouse
809 harboring both EV- or pMIG-OCA-B-transduced cells. 5, 7 and 10 mice were sacrificed at each
810 timepoint to obtain measurements from spleen. All mice were bled at D8, and remaining mice were
811 bled at subsequent timepoints.
812 E) Mean ratios of pMIG-OCA-B-transduced relative to empty vector-transduced SMARTA cells (OCA-
813 B/EV) are plotted. Splenic (top) and peripheral blood (bottom) SMARTA T cells are shown at day 8
814 post-infection, or 7 days post-rechallenge with Lm-gp61 (52+7 or 110+7).
815 F) Flow cytometry showing relative percentages of splenic GFP^+CD44^{hi} EV-transduced (blue) or
816 pMIG-OCAB-transduced (red) SMARTA cells expressing ICOS, PD-1, Ly6C or CD62L at day 8 post-
817 infection. Representative data showing the two populations of cells within a single mouse are shown
818 at day 8 post-infection.
819 G) Percent expression for ICOS, PD-1, CD62L and Ly6C was quantified from four mice using splenic
820 EV- and pMIG-OCAB-transduced GFP^+CD44^{hi} SMARTA cells at 8 days post-infection. Four replicates
821 were performed. For CD26L, the four datapoints are superimposed, and for Ly6C two of the
822 datapoints are superimposed. Individual mice are connected by lines.
823
824 **Figure 3. Gene expression changes associated with ectopic OCA-B expression in SMARTA**
825 **transgenic primary effector T cells.**
826 A) Heatmap showing top up- and down-regulated genes. Genes with log2 fold-change >0.5 or <-1.0,
827 and padj $\leq$ 0.05 are shown. Example genes are shown at right. Control and OCA-B-transduced cells
828 were purified from the same mice using magnetic isolation and FACS.
829 B) Example genome tracks showing two up-regulated genes, *Socs2* and *Gadd45b*. *Pou2af1* (*Ocab*) is
830 shown as a positive control.
831 C) Top Epigenomic roadmap and Molecular function GO terms for the set of OCA-B up- and down-
832 regulated genes.
833 D) Top ChIP-X Enrichment Analysis (ChEA 2016) factors potentially regulating the same set of genes
834 up- and down-regulated by OCA-B ectopic expression.
835
836 **Figure 4. Single-cell RNA-seq analysis of SMARTA cells transduced with OCA-B or empty**
837 **vector.**
838 A) UMAP projections of independently clustered empty vector-transduced (GFP^+) SMARTA cells
839 purified similar to Figures 2 and 3, and subjected to scRNA-seq. Cluster identities were annotated

using a combination of gene expression enrichment (Table S5), cluster identity predictor ImmGen identity scores (Table S6) and PanglaoDB annotation terms. Clusters 1 and 4 were associated with memory formation. Top PanglaoDB annotation terms for cluster 4 are shown below.

B) Similar UMAP projection using OCA-B-transduced cells purified from the same mice as in (A). Cluster identities were annotated similarly to (A). Cluster 3 in OCA-B-transduced cells was most strongly associated with memory formation. Top PanglaoDB annotation terms for cluster 3 are shown below.

C) Feature plots highlighting expression of representative genes for the two UMAP projections in (A) and (B).

D) UMAP projections of the the EV- and OCA-B-transduced single-cell RNA-seq datasets clustered together. For each projection, the percentage of each cluster relative to the total number cells in condition is shown. Cluster identities were annotated using a combination of gene expression enrichment (Table S7), cluster identity predictor ImmGen identity scores and PanglaoDB annotation terms.

E) Feature plots highlighting expression of representative genes for the combined projections.

F) Violin plots depicting expression of six genes (*Il7r*, *Zeb2*, *Gadd45b*, *Foxo1*, *Tcf7* and *Tox*) across each of the 10 clusters in EV-transduced cells (blue, left) and OCA-B-transduced cells (red, right).

Figure 5. mCherry expression in splenic T cell populations in specific pathogen-free homozygous OCA-B-3×mCherry mice.

A) CD4 and CD8 expression are shown for an allelic series of example wild-type (+/+), heterozygous (+/KI) and homozygous OCA-B knock-in reporter mice.

B) OCA-B reporter expression in splenic B cells using the same allelic series of mice as in (A). A more complete analysis of B cell populations is shown in Figure S5.

C) OCA-B reporter expression in splenic $CD4^+$ T cell populations from the same allelic series as in (A).

D) The same $CD4^+$ cells as in (C) were further stratified by CD62L and CD44 into naïve effector (Teff) and central memory (Tcm) populations. $CD62L^{lo}CD44_{lo}$ cells are likely recently activated cells that have down-regulated CD62L but not yet up-regulated CD44.

E) Similar analysis as in (D) except for $CD8^+$ cells.

Figure 6. $CD4^+$ T cells expressing high levels of OCA-B reporter activity preferentially form central memory cells.

A) Schematic for assessing contraction of $mCherry^{hi}$ vs. $mCherry^{lo}$ SMARTA T cells following LCMV infection. Congenically marked SMARTA T cells were isolated from donor mice, transferred into naïve

875 secondary recipients and infected with LCMV. At 8 days post-infection, mCherry^{hi} and mCherry^{lo}
876 populations were isolated by FACS. 8×10^5 SMARTA cells were transferred into naïve recipients. After
877 8 days, splenic CD4$^+$Ly5.1$^+$5.2$^+$ SMARTA cells were evaluated by flow cytometry.
878 B) Flow cytometric analysis of SMARTA donor T cells after 8 days in a naïve animal to monitor rates
879 of decline. Representative animals engrafted with mCherry^{lo} (left) or mCherry^{hi} (right) cells are shown.
880 C) Quantification of averaged donor T cell numbers from mice engrafted with mCherry^{lo} or mCherry^{hi}
881 cells. N=7 for the mCherry^{lo} group and N=5 for the mCherry^{hi} group.
882 D) Similar analysis to (C) except quantifying mean mCherry fluorescence intensity.
883 E) Schematic for assessing recall responses of mCherry^{hi} vs. mCherry^{lo} SMARTA T cells following
884 LCMV infection. Congenically marked SMARTA T cells were isolated from donor mice, transferred
885 into naïve secondary recipients and infected with LCMV as in (A). However, mice were allowed to
886 clear LCMV and form memory. After 43 days, mCherry^{hi} and mCherry^{lo} memory T cell populations
887 were isolated by FACS. 1.3×10^4 SMARTA cells were transferred into naïve recipients, which were
888 infected with LCMV one day later. 7 days post-infection, splenic CD4$^+$Ly5.1$^+$5.2$^+$ SMARTA cells were
889 evaluated by flow cytometry.
890 F) Flow cytometric analysis of SMARTA donor T cells 7 days post-rechallenge to monitor recall
891 responses. Representative animals engrafted with mCherry^{lo} (left) or mCherry^{hi} (right) cells are
892 shown.
893 G) Quantification of averaged donor T cell percentages and numbers from mice engrafted with
894 mCherry^{lo} or mCherry^{hi} cells. N=7 for the mCherry^{lo} group and N=5 for the mCherry^{hi} group.
895 H) Similar analysis to (G) except quantifying mean mCherry fluorescence intensity.
896
897 **Supplemental Figures**
898 **Figure S1, related to Figure 1. Surface marker expression in polyclonal OCA-B T cell-deficient**
899 **and control splenic CD4$^+$ effector T cells at 8 days post-infection or 7 days post-rechallenge.**
900 Example flow cytometry panels of ICOS, Ly6C, CD62L. PD-1 was additionally performed for memory
901 recall responses. Cells were gated for I-A^b-LCMV$^{gp66-77}$ positivity.
902
903 **Figure S2, related to Figure 2. Bulk RNA-seq replicate correlations and example genome**
904 **tracks.**
905 Euclidian distance clustering of bulk RNA-seq replicates to show divergence between replicates and
906 conditions.
907
908 **Figure S3, related to Figure 4. Quality control *Cd3e* and *Cd4* mRNA expression in separately**
909 **clustered single-cell RNA-seq.**

910 A) Feature plots showing gene expression intensities for *Cd3e* (top) and *Cd4* (bottom) in EV-
911 transduced (left) and OCA-B-transduced (right) SMARTA T cells at day 8 post-infection with LCMV.
912 B) Violin plots showing *Cd4* gene expression by cluster for each condition.
913
914 **Figure S4, related to Figure 5. OCA-B-3×mCherry knock-in reporter mice.**
915 A) Mouse *Pou2af*1 locus, targeting vector and the targeted *Pou2af1* locus.
916 B) PCR genotyping OCAB-3×mCherry reporter mice. PCR yields a 494 bp product for the wild-type
917 *Pou2af1* allele and a 373 bp product for targeted *Pou2af1* allele. +=wild-type allele. KI=knock-in allele.
918 C) OCA-B immunoblot using splenocytes from wild-type (+/+) and heterozygous (+/KI) or homozygous
919 knock-in OCAB-3×mCherry knock-in mice. β-actin was used as a loading control.
920 D) Flow cytometry showing mCherry expression in peripheral blood cells of wild-type mice (+/+), or
921 either heterozygous (+/KI) or homozygous (KI/KI) OCAB-3×mCherry knock-in reporter mice.
922 E) Similar flow cytometry plots as in (D) except gated on the indicated populations.
923
924 **Figure S5, related to Figure 5. Characterization OCA-B expression in different B cell**
925 **populations using heterozygous reporter mice.**
926 A) mCherry (OCA-B) expression in a 4.5 week-old heterozygous female OCA-B-3×mCherry reporter
927 mouse. Cells were harvested from bone marrow (BM), peritoneal cavity (PC), spleen (SP), lymph
928 node (LN) or thymus. After removal of red blood cells, mCherry expression was measured in total cell
929 populations.
930 B) Wild-type (+/+) and heterozygous knock-in (+/KI) bone marrow cells were further stratified into B1
931 and B2 populations based on B220 and IgM expression Top plots show relative proportions of B1
932 ($IgM^{hi}B220^{lo}$) B2 ($IgM^{lo}B220^{hi}$) cells in wild-type and two example heterozygous reporter mice. Bottom
933 plots show mCherry expression in gated populations.
934 C) Analysis of peritoneal cavity B cell populations from +/+ and +/KI reporter mice. Cells were
935 stratified into pro/pre, immature and recirculating B cell compartments based on B220 and IgM
936 expression. Top plots show relative proportions of the cells in animals of the indicated genotypes.
937 Bottom plots show mCherry levels in the gated populations.
938 D) Splenic transitional B cells were stratified using CD93 (AA4.1), CD23 and IgM antibodies. One
939 wild-type and two example heterozygous reporter mice are shown.
940 E) Similar analysis to (D) except using CD21 and CD23 antibodies to visualize follicular and marginal
941 zone B cell populations.
942
943 **Figure S6, related to Figure 5. OCA-B reporter expression in thymocytes.**

944 A) mCherry expression in total B220-negative thymocytes from wild-type (+/+) or homozygous knock-
945 in reporter mice was analyzed by flow cytometry. Specific pathogen-free mice were used.
946 B) Thymocytes were stained with CD4 and CD8 antibodies to visualize double-negative, double-
947 positive and single-positive T cell developmental stages in homozygous knock-in reporter mice. Right:
948 mCherry expression in developing reporter T cells was subdivided by quadrant.
949
950 **Figure S7, related to Figure 5. OCA-B reporter expression in total splenic CD4$^+$ and CD8$^+$ T**
951 **cells.**
952 A) mCherry expression was tested in spleens from 9 week-old male homozygous knock-in reporter
953 mice. Specific pathogen-free mice were used.
954 B) mCherry mean fluorescence intensity was calculated from four 9 week-old male homozygous
955 knock-in reporter mice using flow cytometry and gating identical to Figure 5D and E.
956
957 **Figure S8, related to Figure 6. OCA-B reporter expression in antigen-responsive T cells**
958 **following LCMV infection.**
959 A) Flow cytometry images are shown of homozygous OCA-B-3×mCherry knock-in reporter mice at
960 different timepoints following LCMV infection (D0-43) and following rechallenge with Lm-gp61. Mice
961 were challenged on different days and spleens were harvested and processed on the same day. Top
962 panels: percentages of cells expressing CD44 and class II LCMV tetramer (I-A^b LCMV$^{gp66-77}$) are
963 shown. Bottom panels: for the same timepoints cells gated from each quadrant in the top panels are
964 plotted. Each flow panel is representative of biological duplicate mice sacrificed at each timepoint.
965 B) Cells from the same mice as above were gated for CD8 expression and stained with class I LCMV
966 tetramers (H2-D^b LCMV$^{gp33-41}$). Analysis of recall response timepoints was not possible for antigen-
967 specific CD8 cells because animals were rechallenged with Lm-gp61, which lacks CD8
968 immunodominant epitopes.
969
970 **Supplemental Tables**
971
972 **Table S1, related to Figure 3. Differentially expressed bulk RNAseq genes comparing GFP$^+$**
973 **SMARTA T cells expressing empty vector or OCA-B at day 8 post-LCMV infection (cutoffs: -**
974 **1>log2FC>0.5, *p*<0.05).**
975
976 **Table S2, related to Figure 3. Gene Ontology analysis using differentially expressed bulk RNA-**
977 **seq transcripts comparing GFP$^+$ SMARTA T cells transduced with empty vector or OCA-B at**
978 **day 8 post-LCMV infection (cutoffs: -1>log2FC>0.5, *p*<0.05).**

979

980 **Table S3, related to Figure 3. Intersection of differentially expressed bulk RNAseq genes**
981 **comparing GFP$^+$ SMARTA T cells transduced with OCA-B relative to empty vector at 8 days**
982 **post-LCMV infection (cutoffs: -1>log2FC>0.5, *p*<0.05) with differentially expressed genes in**
983 **restimulated T cells lacking OCA-B, published previously (Shakya et al. 2015).**
984

985 **Table S4, related to Figure 3. Intersection between previously published Oct1/OCA-B targets**
986 **(Shakya et al. 2015, 3173 targets*) and bulk RNA-seq comparing GFP$^+$ SMARTA T cells**
987 **transduced with empty vector or OCA-B at day 8 post post-LCMV infection (cutoffs: -**
988 **1>log2FC>0.5, *p*<0.05).**
989

990 **Table S5, related to Figure 4. Single-cell RNA-seq gene enrichments by cluster in GFP$^+$**
991 **SMARTA T cells transduced with empty vector or OCA-B at day 8 post-LCMV infection.**
992

993 **Table S6, related to Figure 4. Top 5 single-cell RNA-seq ImmGen identity scores per cluster**
994 **using GFP$^+$ SMARTA T cells transduced with empty vector or OCA-B at day 8 post-LCMV**
995 **infection.**
996

997 **Table S7, related to Figure 4. Integrated gene enrichment analysis of single-cell RNA-seq gene**
998 **enrichments by cluster in GFP$^+$ SMARTA T cells transduced with empty vector or OCA-B at**
999 **day 8 post-LCMV infection.**

1000 **References**

1001

1002 Ahmed, R., Salmi, A., Butler, L.D., Chiller, J.M., and Oldstone, M.B. (1984). Selection of genetic
1003 variants of lymphocytic choriomeningitis virus in spleens of persistently infected mice. Role in
1004 suppression of cytotoxic T lymphocyte response and viral persistence. J Exp Med *160*, 521-540.
1005 10.1084/jem.160.2.521.
1006 Ban, M., Booth, D., Heard, R., Stewart, G., Goris, A., Vandenbroeck, K., Dubois, B., Laaksonen, M.,
1007 Ilonen, J., Alizadeh, M., et al. (2006). Linkage disequilibrium screening for multiple sclerosis implicates
1008 JAG1 and POU2AF1 as susceptibility genes in Europeans. J Neuroimmunol *179*, 108-116.
1009 Banerjee, A., Gordon, S.M., Intlekofer, A.M., Paley, M.A., Mooney, E.C., Lindsten, T., Wherry, E.J.,
1010 and Reiner, S.L. (2010). Cutting edge: The transcription factor eomesodermin enables CD8+ T cells
1011 to compete for the memory cell niche. J Immunol *185*, 4988-4992. jimmunol.1002042 [pii]
1012 10.4049/jimmunol.1002042 [doi].
1013 Betzler, A.C., Fiedler, K., Hoffmann, T.K., Fehling, H.J., Wirth, T., and Brunner, C. (2022).
1014 BOB.1/OBF.1 is required during B-cell ontogeny for B-cell differentiation and germinal center function.
1015 Eur J Immunol *52*, 404-417. 10.1002/eji.202149333.
1016 Blattman, J.N., Antia, R., Sourdive, D.J., Wang, X., Kaech, S.M., Murali-Krishna, K., Altman, J.D., and
1017 Ahmed, R. (2002). Estimating the precursor frequency of naive antigen-specific CD8 T cells. J Exp
1018 Med *195*, 657-664. 10.1084/jem.20001021.
1019 Cafri, G., Yossef, R., Pasetto, A., Deniger, D.C., Lu, Y.C., Parkhurst, M., Gartner, J.J., Jia, L., Ray, S.,
1020 Ngo, L.T., et al. (2019). Memory T cells targeting oncogenic mutations detected in peripheral blood of
1021 epithelial cancer patients. Nat Commun *10*, 449. 10.1038/s41467-019-08304-z.
1022 Casellas, R., Jankovic, M., Meyer, G., Gazumyan, A., Luo, Y., Roeder, R., and Nussenzweig, M.
1023 (2002). OcaB Is Required for Normal Transcription and V(D)J Recombination of a Subset of
1024 Immunoglobulin kappa Genes. Cell *110*, 575.
1025 Chee, J., Ko, H.J., Skowera, A., Jhala, G., Catterall, T., Graham, K.L., Sutherland, R.M., Thomas,
1026 H.E., Lew, A.M., Peakman, M., et al. (2014). Effector-memory T cells develop in islets and report islet
1027 pathology in type 1 diabetes. J Immunol *192*, 572-580.
1028 Chevrier, S., Kratina, T., Emslie, D., Karnowski, A., and Corcoran, L.M. (2014). Germinal center-
1029 independent, IgM-mediated autoimmunity in sanroque mice lacking Obf1. Immunol Cell Biol *92*, 12-
1030 19.
1031 Ciucci, T., Vacchio, M.S., Gao, Y., Tomassoni Ardori, F., Candia, J., Mehta, M., Zhao, Y., Tran, B.,
1032 Pepper, M., Tessarollo, L., et al. (2019). The Emergence and Functional Fitness of Memory CD4(+) T
1033 Cells Require the Transcription Factor Thpok. Immunity *50*, 91-105 e104.
1034 10.1016/j.immuni.2018.12.019.
1035 Crawford, A., Angelosanto, J.M., Kao, C., Doering, T.A., Odorizzi, P.M., Barnett, B.E., and Wherry,
1036 E.J. (2014). Molecular and transcriptional basis of CD4(+) T cell dysfunction during chronic infection.
1037 Immunity *40*, 289-302. 10.1016/j.immuni.2014.01.005.
1038 Elyaman, W., Kivisakk, P., Reddy, J., Chitnis, T., Raddassi, K., Imitola, J., Bradshaw, E., Kuchroo,
1039 V.K., Yagita, H., Sayegh, M.H., and Khoury, S.J. (2008). Distinct functions of autoreactive memory
1040 and effector CD4+ T cells in experimental autoimmune encephalomyelitis. Am J Pathol *173*, 411-422.
1041 10.2353/ajpath.2008.080142.
1042 Guan, T., Dominguez, C.X., Amezquita, R.A., Laidlaw, B.J., Cheng, J., Henao-Mejia, J., Williams, A.,
1043 Flavell, R.A., Lu, J., and Kaech, S.M. (2018). ZEB1, ZEB2, and the miR-200 family form a
1044 counterregulatory network to regulate CD8(+) T cell fates. J Exp Med *215*, 1153-1168.
1045 10.1084/jem.20171352.
1046 Hess Michelini, R., Doedens, A.L., Goldrath, A.W., and Hedrick, S.M. (2013). Differentiation of CD8
1047 memory T cells depends on Foxo1. J Exp Med *210*, 1189-1200. jem.20130392 [pii]
1048 10.1084/jem.20130392 [doi].
1049 Hurton, L.V., Singh, H., Najjar, A.M., Switzer, K.C., Mi, T., Maiti, S., Olivares, S., Rabinovich, B., Huls,
1050 H., Forget, M.A., et al. (2016). Tethered IL-15 augments antitumor activity and promotes a stem-cell

1051 memory subset in tumor-specific T cells. Proc Natl Acad Sci U S A *113*, E7788-e7797.
1052 10.1073/pnas.1610544113.
1053 Ichii, H., Sakamoto, A., Arima, M., Hatano, M., Kuroda, Y., and Tokuhisa, T. (2007). Bcl6 is essential
1054 for the generation of long-term memory CD4+ T cells. Int Immunol *19*, 427-433. dxm007 [pii]
1055 10.1093/intimm/dxm007 [doi].

1056 Joshi, N.S., Cui, W., Chandele, A., Lee, H.K., Urso, D.R., Hagman, J., Gapin, L., and Kaech, S.M.
1057 (2007). Inflammation directs memory precursor and short-lived effector CD8(+) T cell fates via the
1058 graded expression of T-bet transcription factor. Immunity *27*, 281-295.
1059 Ju, S., Zhu, Y., Liu, L., Dai, S., Li, C., Chen, E., He, Y., Zhang, X., and Lu, B. (2009). Gadd45b and
1060 Gadd45g are important for anti-tumor immune responses. Eur J Immunol *39*, 3010-3018.
1061 10.1002/eji.200839154.
1062 Kallies, A., Xin, A., Belz, G.T., and Nutt, S.L. (2009). Blimp-1 transcription factor is required for the
1063 differentiation of effector CD8(+) T cells and memory responses. Immunity *31*, 283-295.
1064 Kawakami, N., Odoardi, F., Ziemssen, T., Bradl, M., Ritter, T., Neuhaus, O., Lassmann, H., Wekerle,
1065 H., and Flugel, A. (2005). Autoimmune CD4+ T cell memory: lifelong persistence of encephalitogenic
1066 T cell clones in healthy immune repertoires. J Immunol *175*, 69-81.
1067 Kim, C., Jay, D.C., and Williams, M.A. (2012). Stability and function of secondary Th1 memory cells
1068 are dependent on the nature of the secondary stimulus. J Immunol *189*, 2348-2355.
1069 10.4049/jimmunol.1200244.
1070 Kim, H., Dickey, L., Stone, C., Jafek, J.L., Lane, T.E., and Tantin, D. (2019). T cell-selective deletion
1071 of Oct1 protects animals from autoimmune neuroinflammation while maintaining neurotropic pathogen
1072 response. J. Neuroinflamm. *16*. ARTN 133 10.1186/s12974-019-1523-3.
1073 Kim, H., Perovanovic, J., Shakya, A., Shen, Z., German, C.N., A., I., Jafek, J.L., Lin, N.-P., Evavold,
1074 B.D., Chou, D.H., et al. (2021). Targeting OCA-B/Pou2af1 blocks activated, autoreactive T cells in the
1075 pancreas and type-1 diabetes. J Exp Med *218*, e20200533. 10.1084/jem.20200533.
1076 Kim, U., Qin, X.F., Gong, S., Stevens, S., Luo, Y., Nussensweig, M., and Roeder, R.G. (1996). The B-
1077 cell-specific transcription coactivator OCA-B/OBF-1/Bob-1 is essential for normal production of
1078 immunoglobulin isotypes. Nature *383*, 542-547.
1079 Lachmann, A., Xu, H., Krishnan, J., Berger, S.I., Mazloom, A.R., and Ma'ayan, A. (2010). ChEA:
1080 transcription factor regulation inferred from integrating genome-wide ChIP-X experiments.
1081 Bioinformatics *26*, 2438-2444. 10.1093/bioinformatics/btq466.
1082 Laidlaw, B.J., Craft, J.E., and Kaech, S.M. (2016). The multifaceted role of CD4(+) T cells in CD8(+) T
1083 cell memory. Nat Rev Immunol *16*, 102-111. 10.1038/nri.2015.10.
1084 Liu, L., Tran, E., Zhao, Y., Huang, Y., Flavell, R., and Lu, B. (2005). Gadd45 beta and Gadd45
1085 gamma are critical for regulating autoimmunity. J Exp Med *202*, 1341-1347. 10.1084/jem.20051359.
1086 Love, M.I., Huber, W., and Anders, S. (2014). Moderated estimation of fold change and dispersion for
1087 RNA-seq data with DESeq2. Genome Biol *15*, 550.
1088 Lu, X., Chu, C.S., Fang, T., Rayon-Estrada, V., Fang, F., Patke, A., Qian, Y., Clarke, S.H., Melnick,
1089 A.M., Zhang, Y., et al. (2019). MTA2/NuRD Regulates B Cell Development and Cooperates with
1090 OCA-B in Controlling the Pre-B to Immature B Cell Transition. Cell Rep *28*, 472-485 e475.
1091 10.1016/j.celrep.2019.06.029.
1092 Luo, Y., Boyle, D.L., Hammaker, D., Edgar, M., Franzoso, G., and Firestein, G.S. (2011). Suppression
1093 of collagen-induced arthritis in growth arrest and DNA damage-inducible protein 45beta-deficient
1094 mice. Arthritis Rheum *63*, 2949-2955. 10.1002/art.30497.
1095 Luo, Y., and Roeder, R.G. (1995). Cloning, functional characterization, and mechanism of action of
1096 the B-cell-specific transcriptional coactivator OCA-B. Mol. Cell. Biol. *15*, 4115-4124.
1097 Marshall, H.D., Chandele, A., Jung, Y.W., Meng, H., Poholek, A.C., Parish, I.A., Rutishauser, R., Cui,
1098 W., Kleinstein, S.H., Craft, J., and Kaech, S.M. (2011). Differential expression of Ly6C and T-bet
1099 distinguish effector and memory Th1 CD4(+) cell properties during viral infection. Immunity *35*, 633-
1100 646.
1101 Michalek, R.D., Gerriets, V.A., Jacobs, S.R., Macintyre, A.N., MacIver, N.J., Mason, E.F., Sullivan,
1102 S.A., Nichols, A.G., and Rathmell, J.C. (2011). Cutting edge: distinct glycolytic and lipid oxidative

1103 metabolic programs are essential for effector and regulatory CD4+ T cell subsets. J Immunol *186*,
1104 3299-3303. 10.4049/jimmunol.1003613.
1105 Mitchell, D.M., Ravkov, E.V., and Williams, M.A. (2010). Distinct roles for IL-2 and IL-15 in the
1106 differentiation and survival of CD8+ effector and memory T cells. J Immunol *184*, 6719-6730.
1107 jimmunol.0904089 [pii] 10.4049/jimmunol.0904089 [doi].
1108 Murali-Krishna, K., Altman, J.D., Suresh, M., Sourdive, D.J., Zajac, A.J., Miller, J.D., Slansky, J., and
1109 Ahmed, R. (1998). Counting antigen-specific CD8 T cells: a reevaluation of bystander activation
1110 during viral infection. Immunity *8*, 177-187. 10.1016/s1074-7613(00)80470-7.
1111 Nakamura, M., Nishida, N., Kawashima, M., Aiba, Y., Tanaka, A., Yasunami, M., Nakamura, H.,
1112 Komori, A., Nakamuta, M., Zeniya, M., et al. (2012). Genome-wide association study identifies
1113 TNFSF15 and POU2AF1 as susceptibility loci for primary biliary cirrhosis in the Japanese population.
1114 Am J Hum Genet *91*, 721-728.
1115 Nielsen, P.J., Georgiev, O., Lorentz, B., and Schaffner, W. (1996). B lymphocytes are impaired in
1116 mice lacking the transcriptional co-activator Bob1/OCA-B/OBF1. Eur J Immunol *26*, 3214-3218.
1117 Omilusik, K.D., Best, J.A., Yu, B., Goossens, S., Weidemann, A., Nguyen, J.V., Seuntjens, E.,
1118 Stryjewska, A., Zweier, C., Roychoudhuri, R., et al. (2015). Transcriptional repressor ZEB2 promotes
1119 terminal differentiation of CD8+ effector and memory T cell populations during infection. J Exp Med
1120 *212*, 2027-2039. 10.1084/jem.20150194.
1121 Oxenius, A., Bachmann, M.F., Zinkernagel, R.M., and Hengartner, H. (1998). Virus-specific MHC-
1122 class II-restricted TCR-transgenic mice: effects on humoral and cellular immune responses after viral
1123 infection. Eur J Immunol *28*, 390-400.
1124 Pace, L., Goudot, C., Zueva, E., Gueguen, P., Burgdorf, N., Waterfall, J.J., Quivy, J.P., Almouzni, G.,
1125 and Amigorena, S. (2018). The epigenetic control of stemness in CD8(+) T cell fate commitment.
1126 Science *359*, 177-186. 10.1126/science.aah6499.
1127 Pearce, E.L., Walsh, M.C., Cejas, P.J., Harms, G.M., Shen, H., Wang, L.S., Jones, R.G., and Choi, Y.
1128 (2009). Enhancing CD8 T-cell memory by modulating fatty acid metabolism. Nature *460*, 103-107.
1129 nature08097 [pii] 10.1038/nature08097 [doi].
1130 Pepper, M., Pagan, A.J., Igyarto, B.Z., Taylor, J.J., and Jenkins, M.K. (2011). Opposing signals from
1131 the Bcl6 transcription factor and the interleukin-2 receptor generate T helper 1 central and effector
1132 memory cells. Immunity *35*, 583-595.
1133 Perovanovic, J., Wu, Y., Abewe, H., Shen, Z., Hughes, E., Gertz, J., Chandrasekharan, M.B., and
1134 Tantin, D. Oct1 recruits the histone lysine demethylase Utx to canalize lineage specification.
1135 submitted https://www.biorxiv.org/content/10.1101/2020.12.01.406488v2.
1136 Qin, X.F., Reichlin, A., Luo, Y., Roeder, R.G., and Nussenzweig, M.C. (1998). OCA-B integrates B cell
1137 antigen receptor-, CD40L- and IL 4-mediated signals for the germinal center pathway of B cell
1138 development. EMBO J *17*, 5066-5075.
1139 Rao, R.R., Li, Q., Gubbels Bupp, M.R., and Shrikant, P.A. (2012). Transcription factor Foxo1
1140 represses T-bet-mediated effector functions and promotes memory CD8(+) T cell differentiation.
1141 Immunity *36*, 374-387. S1074-7613(12)00088-X [pii] 10.1016/j.immuni.2012.01.015 [doi].
1142 Raphael, I., Joern, R.R., and Forsthuber, T.G. (2020). Memory CD4(+) T Cells in Immunity and
1143 Autoimmune Diseases. Cells *9*, 531. 10.3390/cells9030531.
1144 Rodriguez-Jimenez, P., Fernandez-Messina, L., Ovejero-Benito, M.C., Chicharro, P., Vera-Tome, P.,
1145 Vara, A., Cibrian, D., Martinez-Fleta, P., Jimenez-Fernandez, M., Sanchez-Garcia, I., et al. (2021).
1146 Growth arrest and DNA damage-inducible proteins (GADD45) in psoriasis. Sci Rep *11*, 14579.
1147 10.1038/s41598-021-93780-x.
1148 Rosato, P.C., Wijeyesinghe, S., Stolley, J.M., Nelson, C.E., Davis, R.L., Manlove, L.S., Pennell, C.A.,
1149 Blazar, B.R., Chen, C.C., Geller, M.A., et al. (2019). Virus-specific memory T cells populate tumors
1150 and can be repurposed for tumor immunotherapy. Nat Commun *10*, 567. 10.1038/s41467-019-08534-
1151 1.
1152 Rutishauser, R.L., Martins, G.A., Kalachikov, S., Chandele, A., Parish, I.A., Meffre, E., Jacob, J.,
1153 Calame, K., and Kaech, S.M. (2009). Transcriptional repressor Blimp-1 promotes CD8(+) T cell
1154 terminal differentiation and represses the acquisition of central memory T cell properties. Immunity *31*,
1155 296-308.

1156 Sallusto, F., Lanzavecchia, A., Araki, K., and Ahmed, R. (2010). From vaccines to memory and back.
1157 Immunity *33*, 451-463. 10.1016/j.immuni.2010.10.008.
1158 Samardzic, T., Marinkovic, D., Nielsen, P.J., Nitschke, L., and Wirth, T. (2002). BOB.1/OBF.1
1159 deficiency affects marginal-zone B-cell compartment. Mol Cell Biol *22*, 8320-8331.
1160 10.1128/MCB.22.23.8320-8331.2002.
1161 Sauter, P., and Matthias, P. (1997). The B cell-specific coactivator OBF-1 (OCA-B, Bob-1) is inducible
1162 in T cells and its expression is dispensable for IL-2 gene induction. Immunobiology *198*, 207-216.
1163 S0171-2985(97)80041-1 [pii] 10.1016/S0171-2985(97)80041-1 [doi].
1164 Schubart, D.B., Rolink, A., Kosco-Vilbois, R.G., Botteri, F., and Matthias, P. (1996). B-cell-specific
1165 coactivator OBF-1/OCA-B/Bob1 required for immune response and germinal centre formation. Nature
1166 *383*, 538-542.
1167 Shakya, A., Goren, A., Shalek, A., German, C.N., Snook, J., Kuchroo, V.K., Yosef, N., Chan, R.C.,
1168 Regev, A., Williams, M.A., and Tantin, D. (2015). Oct1 and OCA-B are selectively required for CD4
1169 memory T cell function. J Exp Med *212*, 2115-2131. 10.1084/jem.20150363.
1170 Shakya, A., Kang, J., Chumley, J., Williams, M.A., and Tantin, D. (2011). Oct1 is a switchable,
1171 bipotential stabilizer of repressed and inducible transcriptional states. J Biol Chem *286*, 450-459.
1172 10.1074/jbc.M110.174045.
1173 Shen, H., Slifka, M.K., Matloubian, M., Jensen, E.R., Ahmed, R., and Miller, J.F. (1995). Recombinant
1174 Listeria monocytogenes as a live vaccine vehicle for the induction of protective anti-viral cell-mediated
1175 immunity. Proc Natl Acad Sci U S A *92*, 3987-3991. 10.1073/pnas.92.9.3987.
1176 Shin, H.M., Kapoor, V., Guan, T., Kaech, S.M., Welsh, R.M., and Berg, L.J. (2013). Epigenetic
1177 modifications induced by Blimp-1 Regulate CD8(+) T cell memory progression during acute virus
1178 infection. Immunity *39*, 661-675. 10.1016/j.immuni.2013.08.032.
1179 Snook, J.P., Kim, C., and Williams, M.A. (2018). TCR signal strength controls the differentiation of
1180 CD4(+) effector and memory T cells. Sci Immunol *3*, eaas9103. 10.1126/sciimmunol.aas9103.
1181 Strubin, M., Newell, J.W., and Matthias, P. (1995). OBF-1, a novel B cell-specific coactivator that
1182 stimulates immunoglobulin promoter activity through association with octamer-binding proteins. Cell
1183 *80*, 497-506.
1184 Stuart, T., Butler, A., Hoffman, P., Hafemeister, C., Papalexi, E., Mauck, W.M., 3rd, Hao, Y.,
1185 Stoeckius, M., Smibert, P., and Satija, R. (2019). Comprehensive Integration of Single-Cell Data. Cell
1186 *177*, 1888-1902 e1821. 10.1016/j.cell.2019.05.031.
1187 Utzschneider, D.T., Charmoy, M., Chennupati, V., Pousse, L., Ferreira, D.P., Calderon-Copete, S.,
1188 Danilo, M., Alfei, F., Hofmann, M., Wieland, D., et al. (2016). T Cell Factor 1-Expressing Memory-like
1189 CD8(+) T Cells Sustain the Immune Response to Chronic Viral Infections. Immunity *45*, 415-427.
1190 10.1016/j.immuni.2016.07.021.
1191 Williams, M.A., Ravkov, E.V., and Bevan, M.J. (2008). Rapid culling of the CD4+ T cell repertoire in
1192 the transition from effector to memory. Immunity *28*, 533-545.
1193 Yeo, L., Woodwyk, A., Sood, S., Lorenc, A., Eichmann, M., Pujol-Autonell, I., Melchiotti, R., Skowera,
1194 A., Fidanis, E., Dolton, G.M., et al. (2018). Autoreactive T effector memory differentiation mirrors beta
1195 cell function in type 1 diabetes. J Clin Invest *128*, 3460-3474.
1196 Zwilling, S., Dieckmann, A., Pfisterer, P., Angel, P., and Wirth, T. (1997). Inducible expression and
1197 phosphorylation of coactivator BOB.1/OBF.1 in T cells. Science *277*, 221-225.

Sun, Kim et al. Figure 1

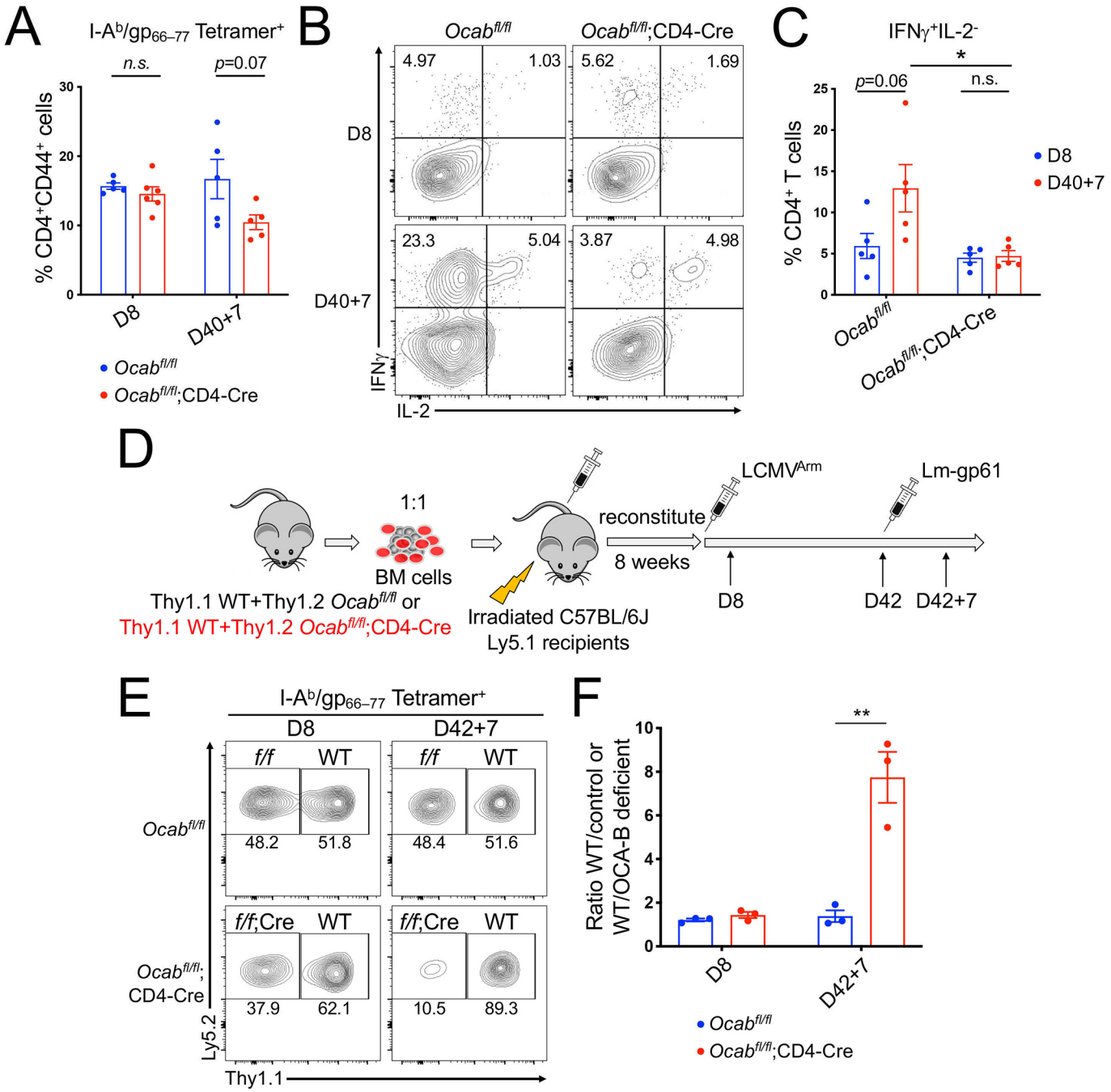

Sun, Kim et al. Figure 2

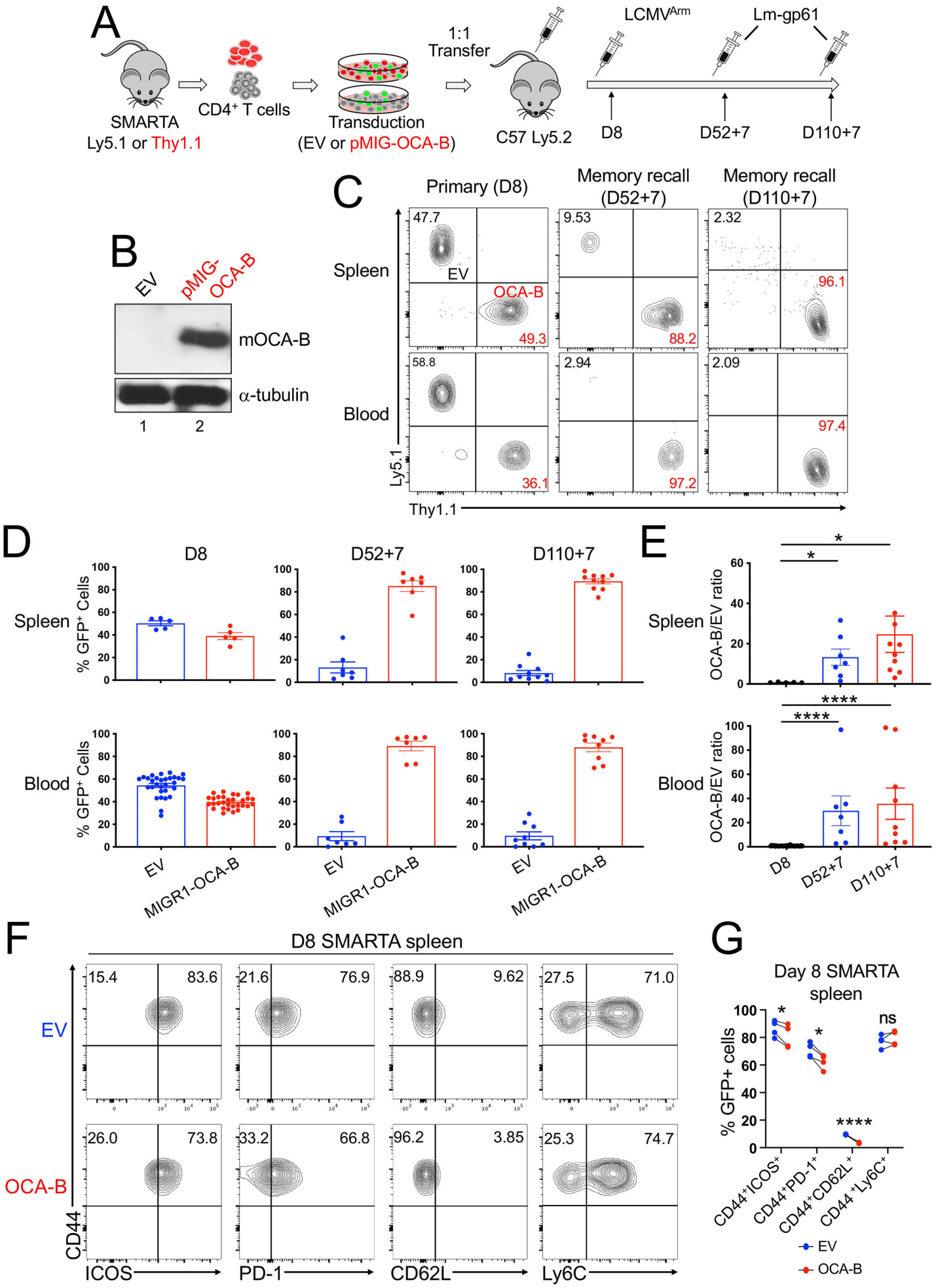

Sun, Kim et al. Figure 3

A

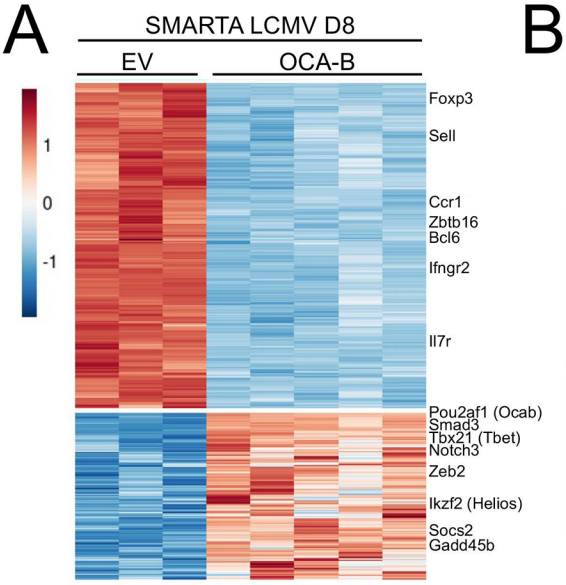

B

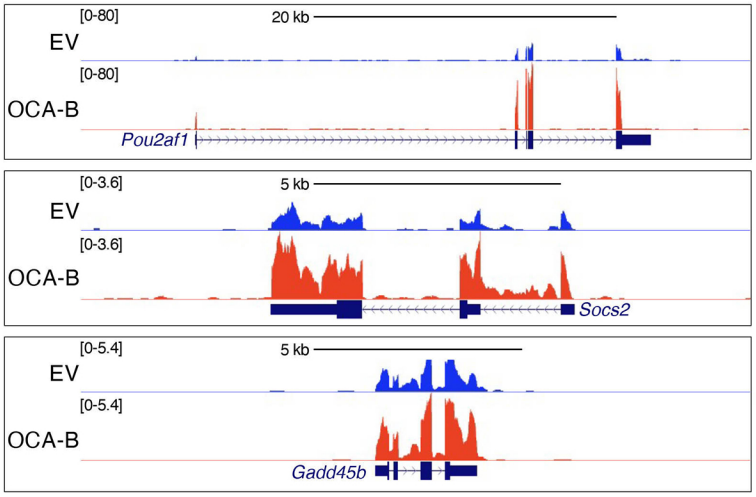

C

OCA-B upregulated genes

Epigenomic roadmap HM	*p*-value
H3K9me3 Breast vHMEC	0.048
Molecular function	***p*-value**
Toll-like receptor binding	0.006
Aspartic-type peptidase activity	0.007

OCA-B downregulated genes

Epigenomic roadmap HM	*p*-value
H3K27me3 CD4 Memory Primary Cells	1.45E-04
H3K27me3 CD8 Memory Primary Cells	9.30E-04
Molecular function	***p*-value**
Superoxide-generating NADPH oxidase activator activity	1.29E-09
Cytokine receptor activity	1.24E-06

D

OCA-B upregulated genes

ChEA 2016	*p*-value
Tp53	0.01936
Smc3	0.02544

OCA-B downregulated genes

ChEA 2016	*p*-value
IRF8	1.24E-20
SMRT	1.14E-15
MYB	1.73E-09
Nerf2	4.79E-09
NCOR	1.52E-08

Sun, Kim et al. Figure 4

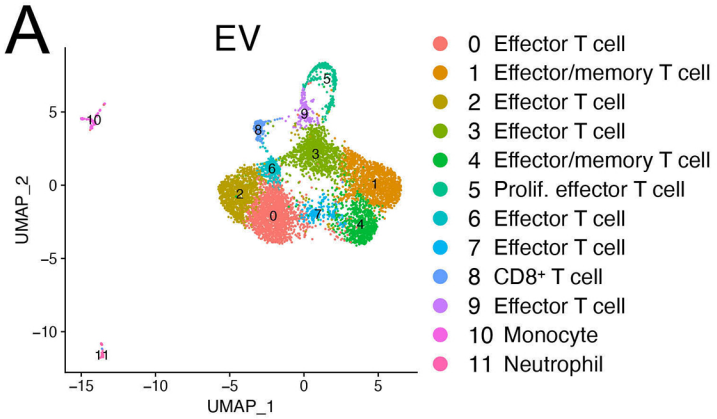

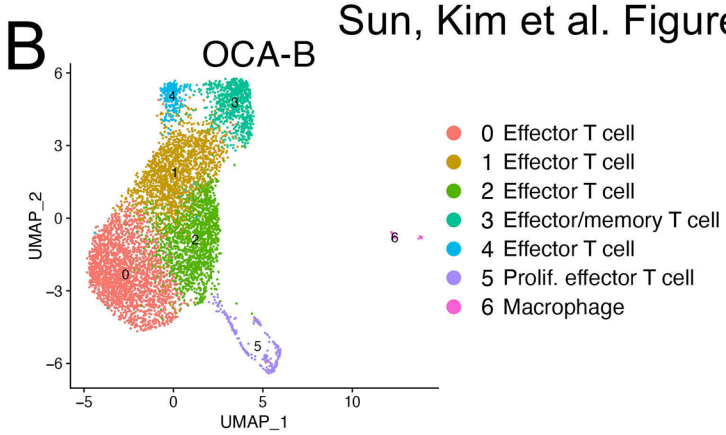

PanglaoDB Augmented 2021 annotation terms

EV Cluster 4	*p*-value
T Memory Cells	3.37E-9
NK Cells	4.25E-5

PanglaoDB Augmented 2021 annotation terms

OE Cluster 3	*p*-value
T Memory Cells	3.45E-7
T Cells	1.77E-6

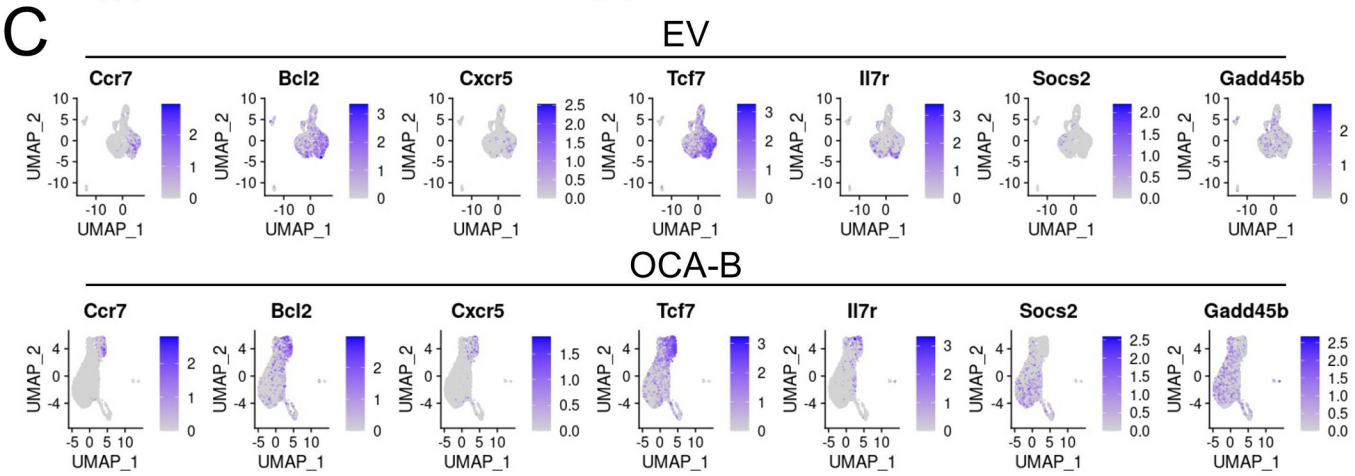

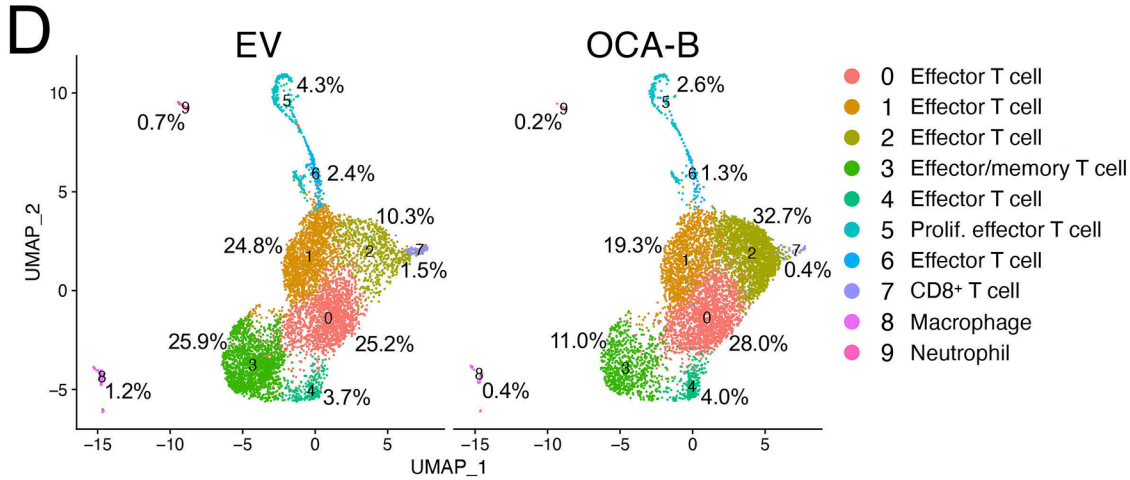

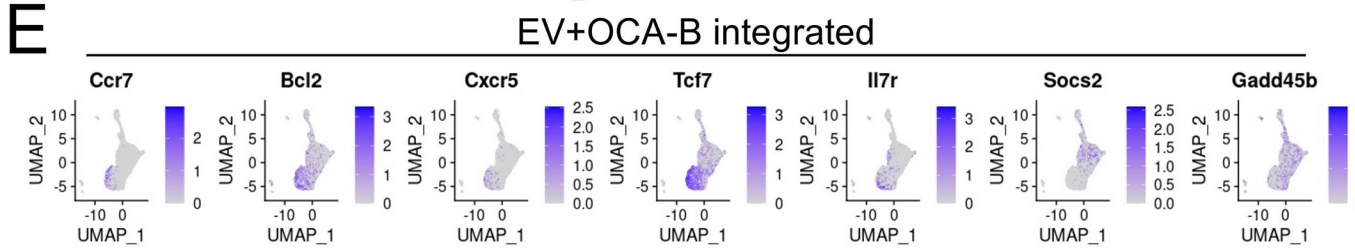

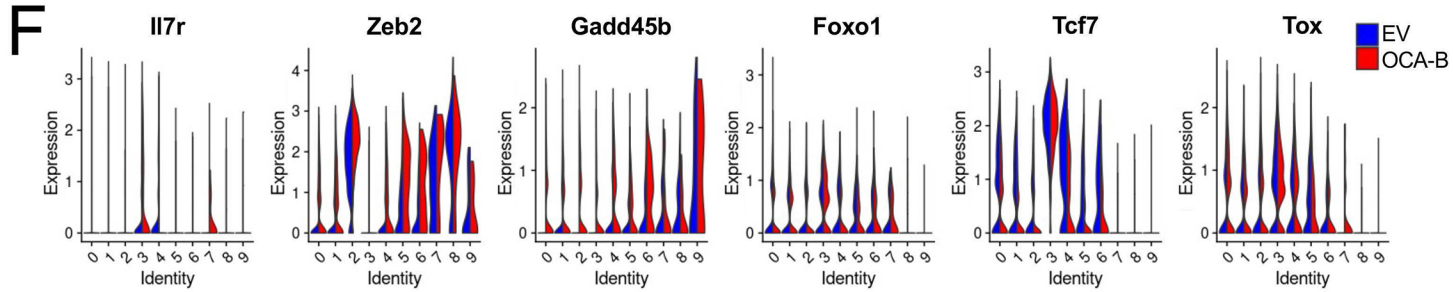

Sun, Kim et al. Figure 5

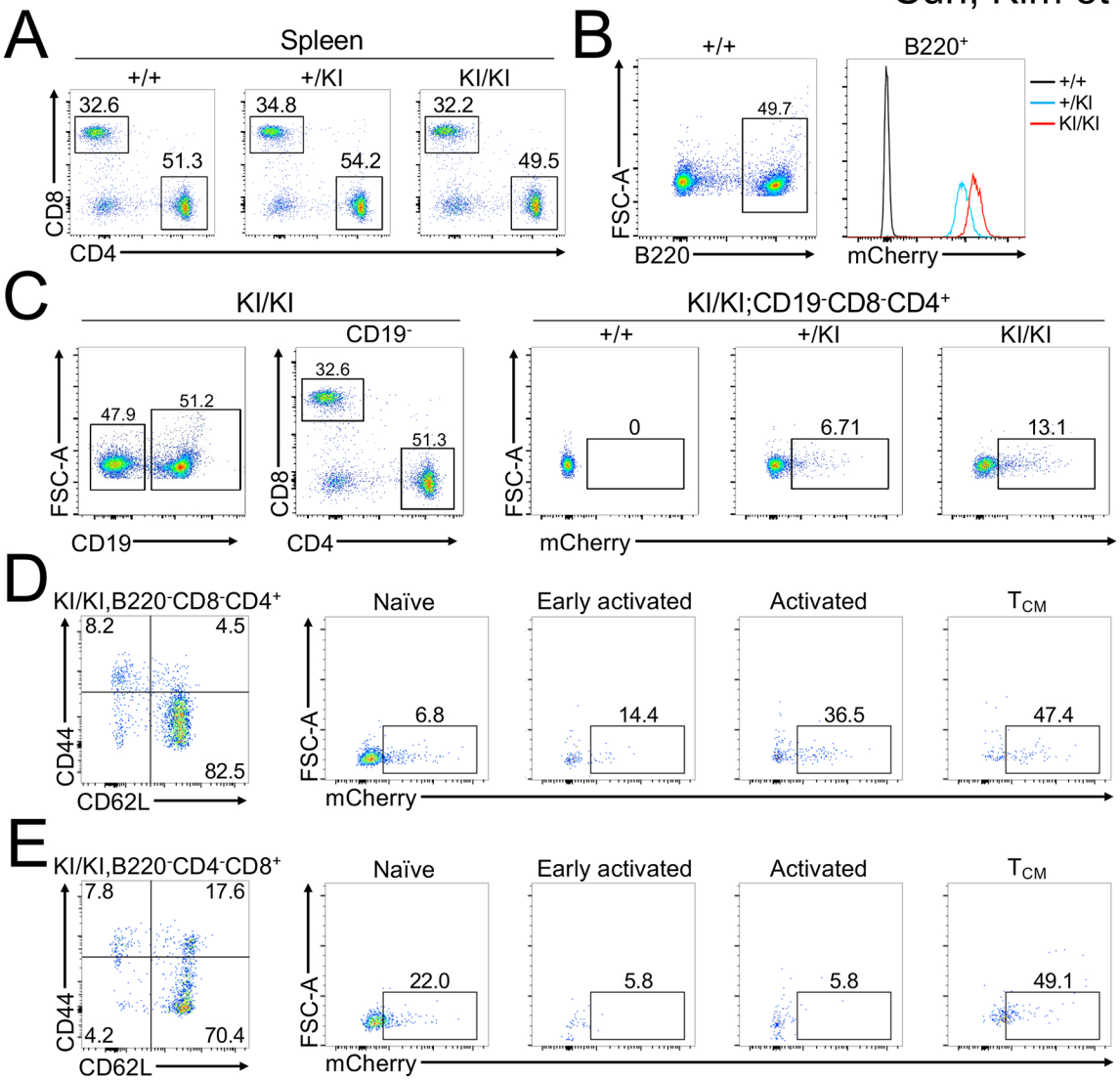
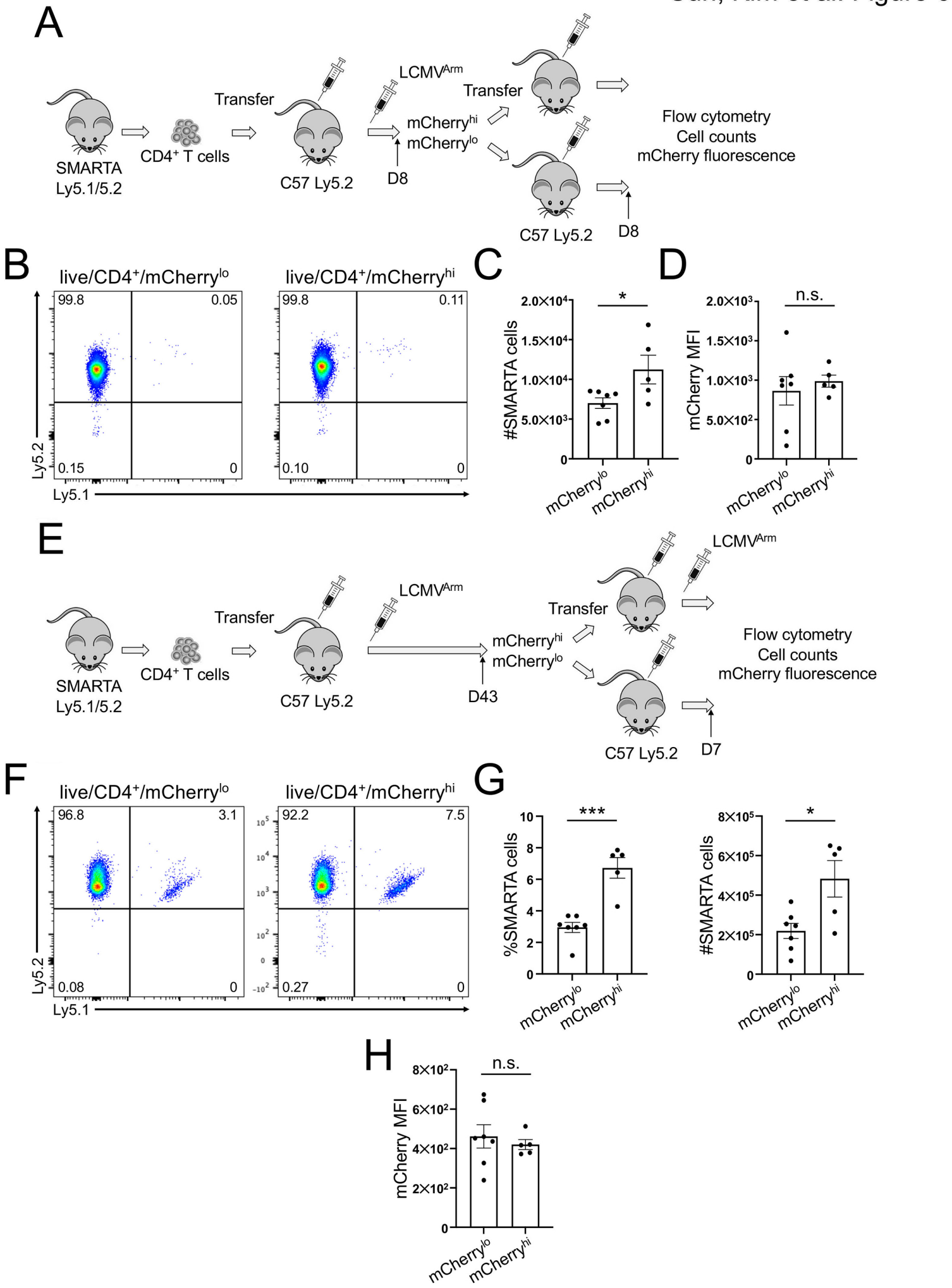
Sun, Kim et al. Figure 6